Role of CAMK2D in neurodevelopment and associated conditions

Authors

Pomme M.F. Rigter, Charlotte de Konink, Matthew J. Dunn, ..., Margaret M. Stratton, Sébastien Küry, Geeske M. van Woerden

Correspondence

sebastien.kury@chu-nantes.fr (S.K.), g.vanwoerden@erasmusmc.nl (G.M.v.W.)

CAMK2 disorder is a relatively new disorder where three of the four CAMK2s (CAMK2A, B, and G) are shown to cause neurodevelopmental disorders. In this paper we describe a cohort of eight individuals with neurodevelopmental disorders and cardiac abnormalities, having CAMK2D variants, proving all CAMK2s are important for normal development.

Rigter et al., 2024, The American Journal of Human Genetics *111*, 364–382
February 1, 2024
https://doi.org/10.1016/j.ajhg.2023.12.016

CellPress

ARTICLE

Role of CAMK2D in neurodevelopment and associated conditions

Pomme M.F. Rigter,[1,2,36] Charlotte de Konink,[2,3,36] Matthew J. Dunn,[4] Martina Proietti Onori,[2,3] Jennifer B. Humberson,[5] Matthew Thomas,[6] Caitlin Barnes,[6] Carlos E. Prada,[7,8,9] K. Nicole Weaver,[10,11] Thomas D. Ryan,[10,12] Oana Caluseriu,[13,14] Jennifer Conway,[15] Emily Calamaro,[16] Chin-To Fong,[16] Wim Wuyts,[17] Marije Meuwissen,[17] Eva Hordijk,[3] Carsten N. Jonkers,[3] Lucas Anderson,[3] Berfin Yuseinova,[3] Sarah Polonia,[1] Diane Beysen,[18,19] Zornitza Stark,[20,21] Elena Savva,[20] Cathryn Poulton,[22] Fiona McKenzie,[22,23] Elizabeth Bhoj,[24] Caleb P. Bupp,[25] Stéphane Bézieau,[26,27] Sandra Mercier,[26,27] Amy Blevins,[28] Ingrid M. Wentzensen,[29] Fan Xia,[29] Jill A. Rosenfeld,[29,30] Tzung-Chien Hsieh,[31] Peter M. Krawitz,[31] Miriam Elbracht,[32] Danielle C.M. Veenma,[2,33] Howard Schulman,[34,35] Margaret M. Stratton,[4] Sébastien Küry,[25,26,*] and Geeske M. van Woerden[1,2,3,*]

Summary

The calcium/calmodulin-dependent protein kinase type 2 (CAMK2) family consists of four different isozymes, encoded by four different genes—*CAMK2A, CAMK2B, CAMK2G*, and *CAMK2D*—of which the first three have been associated recently with neurodevelopmental disorders. CAMK2D is one of the major CAMK2 proteins expressed in the heart and has been associated with cardiac anomalies. Although this CAMK2 isoform is also known to be one of the major CAMK2 subtypes expressed during early brain development, it has never been linked with neurodevelopmental disorders until now. Here we show that CAMK2D plays an important role in neurodevelopment not only in mice but also in humans. We identified eight individuals harboring heterozygous variants in *CAMK2D* who display symptoms of intellectual disability, delayed speech, behavioral problems, and dilated cardiomyopathy. The majority of the variants tested lead to a gain of function (GoF), which appears to cause both neurological problems and dilated cardiomyopathy. In contrast, loss-of-function (LoF) variants appear to induce only neurological symptoms. Together, we describe a cohort of individuals with neurodevelopmental disorders and cardiac anomalies, harboring pathogenic variants in *CAMK2D*, confirming an important role for the CAMK2D isozyme in both heart and brain function.

Introduction

The family of calcium/calmodulin-dependent protein kinase II (CAMK2) mediates calcium-dependent signaling and consists of four members: CAMK2A, CAMK2B, CAMK2G, and CAMK2D. All four proteins are highly homologous and share an evolutionarily conserved structure consisting of a kinase domain, regulatory segment, linker region, and association domain. The kinase domain is the catalytic component and binds ATP; the regulatory domain enforces autoinhibition of kinase activity in the basal state, binds to calcium/calmodulin (Ca^{2+}/CaM), and harbors the Thr286/287 autophosphorylation site, which generates autonomous activity; the linker region (or variable domain) is highly susceptible to alternative splicing and shows the most variability between the

[1]Department of Clinical Genetics, Erasmus Medical Center, Rotterdam 3015 GD, the Netherlands; [2]ENCORE Expertise Centre for Neurodevelopmental Disorders, Erasmus Medical Center, Rotterdam 3015 GD, the Netherlands; [3]Department of Neuroscience, Erasmus Medical Center, Rotterdam 3015 GD, the Netherlands; [4]Department of Biochemistry and Molecular Biology, University of Massachusetts, Amherst, MA 01003, USA; [5]Pediatric Specialty Care, University of Virginia Health, Charlottesville, VA 22903, USA; [6]Division of Genetics, Department of Pediatrics, University of Virginia Children's, Charlottesville, VA 22903, USA; [7]Department of Pediatrics, Northwestern University Feinberg School of Medicine, Chicago, IL 60611, USA; [8]Division of Genetics, Genomics, and Metabolism, Ann & Robert H. Lurie Children's Hospital of Chicago, Chicago, IL 60611, USA; [9]Fundacion Cardiovascular de Colombia, Bucaramanga, Colombia; [10]Department of Pediatrics, University of Cincinnati College of Medicine, Cincinnati, OH 45267, USA; [11]Division of Human Genetics, Cincinnati Children's Hospital Medical Center, Cincinnati, OH 45229, USA; [12]Heart Institute, Cincinnati Children's Hospital Medical Center, Cincinnati, OH 45229, USA; [13]Department of Medical Genetics, University of Alberta, Edmonton, AB T6G 2H7, Canada; [14]Stollery Children's Hospital, Department of Medical Genetics, University of Alberta, Edmonton, AB T6G 2B7, Canada; [15]Stollery Children's Hospital, Department of Pediatrics, Division of Pediatric Cardiology, University of Alberta, Edmonton, AB T6G 2B7, Canada; [16]Department of Pediatrics, University of Rochester School of Medicine and Dentistry, Rochester, NY 14642, USA; [17]Department of Medical Genetics, University of Antwerp and University Hospital of Antwerp, 2650 Edegem, Belgium; [18]Department of Paediatric Neurology, University Hospital of Antwerp, 2650 Edegem, Belgium; [19]Department of Translational Neurosciences, University of Antwerp, 2650 Edegem, Belgium; [20]Victorian Clinical Genetics Services, Murdoch Children's Research Institute, Melbourne, VIC 3052, Australia; [21]Australian Genomics, Melbourne, VIC 3052, Australia; [22]Genetic Services of Western Australia, King Edward Memorial Hospital, Perth, WA 6008, Australia; [23]School of Paediatrics and Child Health, University of Western Australia, Perth, WA 6009, Australia; [24]Division of Human Genetics, Department of Pediatrics, The Children's Hospital of Philadelphia, Philadelphia, PA 19104, USA; [25]Corewell Health & Helen DeVos Children's Hospital, Grand Rapids, MI 49503, USA; [26]Nantes Université, CHU Nantes, Service de Génétique Médicale, 44000 Nantes, France; [27]Nantes Université, CHU Nantes, CNRS, INSERM, l'institut du thorax, 44000 Nantes, France; [28]GeneDx, Gaithersburg, MD 20877, USA; [29]Department of Molecular and Human Genetics, Baylor College of Medicine, Houston, TX 77030, USA; [30]Baylor Genetics Laboratories, Houston, TX 77021, USA; [31]Institute for Genomic Statistics and Bioinformatics, University of Bonn, 53127 Bonn, Germany; [32]Institute for Human Genetics and Genomic Medicine, Medical Faculty, RWTH Aachen University, 52074 Aachen, Germany; [33]Sophia Children's Hospital, Erasmus Medical Center, Rotterdam 3015 CN, the Netherlands; [34]Department of Neurobiology, Stanford University, School of Medicine, Stanford, CA 94305, USA; [35]Panorama Research Institute, Sunnyvale, CA 94089, USA
[36]These authors contributed equally
*Correspondence: sebastien.kury@chu-nantes.fr (S.K.), g.vanwoerden@erasmusmc.nl (G.M.v.W.)
https://doi.org/10.1016/j.ajhg.2023.12.016.

different CAMK2 members; the association domain (or hub domain) is where the same or different CAMK2 molecules oligomerize to form the functional holoenzyme that generally consists of 12–14 subunits.[1–5]

CAMK2's central role in synaptic plasticity, learning, and memory was established in various animal models, with a prime focus on CAMK2A,[6–9] followed by CAMK2B.[10–13] Although these two isozymes have unique functions in the brain, as shown by the phenotypes of the different knockout mouse models, they can also partially compensate for each other's loss. Simultaneous deletion of *Camk2a* and *Camk2b* results in early postnatal lethality in mice, as well as lethality in the adult stage upon adult-induced deletion.[14] Additionally, simultaneous deletion of *Camk2a* and *Camk2b* in the adult completely abolished long-term potentiation (LTP) at the CA3-CA1 synapse in the hippocampus.[14] CAMK2G and CAMK2D are also expressed in the brain, albeit at much lower levels compared to CAMK2A and CAMK2B, and cannot compensate for absence of both CAMK2A and CAMK2B in survival or plasticity despite their high homology. Interestingly, a few recently published studies do point toward an important role for CAMK2G and CAMK2D in learning and memory in addition to their better defined non-neuronal functions.[15–17] In mice, *Camk2g* has been shown to participate in excitation transcription coupling in excitatory neurons and in hippocampal synaptic plasticity in inhibitory neurons.[15,16,18] Moreover, *Camk2g* has been shown to be involved in normal development of neurons and innate behaviors that have been associated with critical windows during development.[19,20] *Camk2d*, on the other hand, is suggested to play a role in long-term memory consolidation, since in mice its RNA levels are upregulated up to seven days after executing a memory task, showing a positive correlation with the mouse's memory performance.[17] Correspondingly, knockdown of *Camk2d* after training impairs memory performance specifically when tested multiple days later.[17]

The importance of CAMK2 in normal human brain functioning has been highlighted by the identification of individuals with neurodevelopmental disorders carrying pathogenic variants in one of the *CAMK2* genes. The first identified variant, discovered by exome sequencing, was located in *CAMK2G* (intellectual developmental disorder, autosomal dominant 59 [MIM: 618522]),[19,21] which is somewhat surprising considering that CAMK2G is much less abundant in the brain, compared to CAMK2A or CAMK2B, but proving a function for this kinase in normal human brain function. Next, cohorts of individuals with neurodevelopmental disorders were identified with causative variants in *CAMK2A* and *CAMK2B* (intellectual developmental disorder, autosomal dominant 53 [MIM: 617798] and 54 [MIM: 617798], respectively).[22–28] For *CAMK2D*, a role in human brain function has not been established thus far.

CAMK2D is expressed in multiple organs, including the brain, but has the highest expression levels in the heart.[29,30] *CAMK2D* has multiple isoforms due to alternative splicing, which can result in different cellular localization.[31] Deep sequencing of human samples of the hippocampus consistently detected six *CAMK2D* splice variants, of which *CAMK2D* (6v1,14b,18) and (6v1,14a,18) were most prevalent[32] (GenBank: XP_047272177.1 and NM_001321571.2, respectively).

The expression pattern of *Camk2d* in rodent brain is widespread, showing elevated levels in granule cells of the cerebellum, a laminar distribution in layers II/III, IV, and deep VI of the cortex, and a global distribution in the cell layers of the hippocampus.[29,33,34] During rodent brain development, *Camk2d* expression can be detected around embryonic day 10 and increases rapidly postnatally.[30,33] It is then expressed in multiple cell types, such as excitatory neurons, interneurons, and astrocytes.[35–37] During human brain development, stable RNA levels are detectable throughout gestation, starting in the first trimester.[19] This expression profile hints at a possible neurodevelopmental role for *CAMK2D*.

In this manuscript, we sought to determine whether CAMK2D indeed plays a role in neurodevelopment. Our data provide evidence for the importance of CAMK2D in neurodevelopment *in vitro* and *in vivo*. Additionally, we present pathogenic variants in the *CAMK2D* gene identified in individuals with neurodevelopmental disorders, confirming its clinical relevance for cognitive function.

Subjects and methods

Genetic identification of the variants

The eight affected individuals participating in the study come from seven unrelated families. They were clinically assessed by centers internationally. All participants presented with unexplained congenital cardiomyopathy and/or developmental delay or intellectual disability. As relevant routine genetic testing, including copy number variation (CNV) analysis by high-resolution array-based comparative genomic hybridization (aCGH), had provided no diagnosis, exome sequencing or genome sequencing was performed in a diagnostic or research setting, which highlighted rare *CAMK2D* candidate variants. Segregation analysis was performed by Sanger or exome/genome sequencing. Contact between participating centers and teams was aided by the web-based tool GeneMatcher.[38] Written informed consent was obtained from each affected individual or her/his guardian and available family members for use of medical history, genetic testing report, and photograph (if applicable), in accordance with the respective human ethics committees of each participating institution. Authorization to publish photographs was obtained from the parents of individuals 1, 2, 4, and 5.

Cloning for the stability assay and the *in vivo* and *in vitro* neuronal experiments

$CAMK2D^{WT}$ sequence (GenBank: NM_001321571.2) was obtained from the human brain cDNA library and immediately tagged with restriction sites AscI and PacI by PCR, which made it possible to ligate the $CAMK2D^{WT}$ sequence into the TOPO vector and our dual promoter expression vector.[19] For the primers used, see

Table S1. For overexpression, single nucleotide variants were introduced in the *CAMK2D*^{WT} sequence in TOPO, using site-directed PCR mutagenesis. For the primers used for mutagenesis, see Table S2. Once successfully mutated, the sequence was ligated into the multiple cloning site (MCS) of the expression vector. The exact same expression vector, lacking an insert in the MCS, was used as a negative control throughout the experiments and referred to as "empty vector control." For knockdown experiments, three different shRNAs that specifically target the coding sequence of mouse *Camk2d*, were obtained from the MISSION shRNA library for mouse genomes of Sigma Life Sciences and The RNAi Consortium (TRC): (1) 5′-GCAACTGATTGAAGCTATCAA-3′; (2) 5′-GCATAGACTGTATCAGCAGAT-3′; (3) 5′-CCTGAAGCATTGGG CAACTTA-3′. The control shRNA plasmid is the MISSION non-target shRNA control vector: 5′-CAACAAGATGAAGAGCACCAA-3′.

HEK293T transfections

Plasmids encoding the different *CAMK2D* variants were transfected in HEK293T cells. These cells were not authenticated. HEK293T cells were cultured in DMEM/10% Fetal Bovine Serum (FBS)/1% penicillin/streptomycin. Transfection was performed at 60%–70% confluency. Each well (6-well plate) was transfected with 3 μg DNA construct. The following constructs were transfected using polyethyleneimine (PEI) in a 1:3 (DNA:PEI) ratio: Empty vector control; *CAMK2D*^{WT}; *CAMK2D*^{S79N}; *CAMK2D*^{P139L}; *CAMK2D*^{G210R}; *CAMK2D*^{Q274P}; *CAMK2D*^{R275H}; *CAMK2D*^{L291F}. To assess the efficiency of the *Camk2d* shRNAs, 2 μg shRNA construct was co-transfected with 1 μg mouse *Camk2d* construct (6v1, 14a, 18; for nomenclature see Sloutsky and Stratton[39]). To test its specificity, co-transfections of the shRNAs were also executed with mouse *Camk2a* (14, 18) and *Camk2b* (13, 14b, 16, 17, 18) plasmids. To avoid toxicity of the PEI, the medium was refreshed 4–6 h post-transfection. Transfected cells were used to prepare protein lysates for western blot.

Sample preparation and immunoblotting

The cultures were incubated for 48–72 h post-transfection, until full confluency. At this point the cells were harvested in ice-cold PBS, by scraping them off the bottom of the wells. After spinning down, the cell pellet was enriched with a mixture of Laemmli buffer (4% SDS, 0.1M Tris [pH 6.8])/protease inhibitor (Cat. nr. P3840, Sigma)/phosphatase inhibitor cocktails 2 and 3 (resp. Cat. nr. P5726, Sigma; Cat. nr. P0044, Sigma). After the samples were briefly sonicated, the concentrations of the protein lysates were measured, using the BCA assay kit (Cat. nr. 23225, Thermo Fisher Scientific). Samples were diluted to a concentration of 1 μg/μL and prepared for loading with DTT and XT Sample buffer (Cat. nr. 1610791, Biorad). 15 μg protein/lane was loaded in precast Bis-Tris 4%–12% gels (Cat. nr. 3450124, Biorad). After running, the proteins were transferred to the nitrocellulose membrane (Cat. nr. 1704159, Biorad) using the TurboBlot (Cat. nr.1704150, Biorad). Membranes were blocked with 5% milk in TBS-T and incubated with primary antibodies: rabbit-*anti*-phThr286/7, 1:2,000 dilution (Cat. nr. ab124880, Abcam); mouse-*anti*-CAMK2D, 1:500 dilution (Cat. nr. sc-100362, Santa Cruz); rabbit-*anti*-RFP, 1:2,000 diluted (Cat. nr. 600-401-379, Rockland), mouse-*anti*-CAMK2A, 1:20,000 diluted (Cat. nr. NB100-1983, Novus Biologicals); mouse-*anti*-CAMK2B, 1:10,000 diluted (Cat. nr. 13-9800, Invitrogen). For visualization with the Odyssey scanning device, secondary antibodies with fluorescent tags were used, 1:15,000 diluted: goat-*anti*-rabbit (Cat. nr. 926-68021, Westburg); goat-*anti*-mouse (Cat. nr. 926-32210, Westburg).

Plasmid construction for the kinase assay

Constructs were built utilizing exon gene blocks (IDT) and pre-existing pSMT3 vectors containing N-terminal 6xHis followed by a SUMO tag and full-length *CAMK2D* variants via Gibson Assembly. Mutants were cloned via site-directed mutagenesis and confirmed via Sanger sequencing (GeneWiz).

CAMK2D expression and purification

A previously established bacterial expression system[40] for *CAMK2D* by co-expression with Lambda Phosphatase was utilized. We expressed *CAMK2D* in *Escherichia coli* by co-expressing with λ phosphatase (from Kuriyan Lab) in Rosetta (DE3)pLysS competent cells (Novagen). λ phosphatase was expressed via a pCDFDuet1 vector and N-terminal tagged clones 6xHis AviTag *CAMK2D* was expressed in a pET287 vector. Cells were grown to an OD (595 nm) of 0.6 and induced with 1 mM isopropyl β-D-1-thiogalactopyranoside (IPTG; GoldBio). Cells were grown for 16 h at 18°C and resuspended in buffer A (25 mM Tris-HCl [pH 8.5], 150 mM KCl, 50 mM imidazole, 10% glycerol; Sigma) with 25 mM magnesium chloride, containing a cocktail of protease inhibitors and deoxyribonuclease (DNase) (0.2 mM 4 benzenesulfonyl fluoride hydrochloride [AEBSF], 5.0 μM leupeptin, pepstatin [1 μg/mL], aprotinin [1 μg/mL], trypsin inhibitor [0.1 mg/mL], 0.5 mM benzamidine, DNase [1 μg/mL]) (Sigma). Resuspended cells were flash frozen until used.

Cells were lysed via a French press, and clarified cell lysate was aspirated from cell debris following centrifugation (18,000 rpm; 4°C; 60 min). All subsequent purification steps were performed with an ÄKTA pure chromatography system (Cytiva Life Sciences) at 4°C. Clarified cell lysate was loaded onto two 5-mL HisTrap FF NiNTA Sepharose columns (Cytiva Life Sciences) and eluted with a combination of 50% buffer A and 50% buffer B (25 mM Tris-HCl [pH 8.5], 150 mM KCl, 1 M imidazole, 10% glycerol) for a final concentration of 0.5 M imidazole. The eluate was desalted of residual imidazole with a HiPrep 26/10 Desalting column, and His SUMO tags were cleaved with Ulp1 protease overnight at 4°C in buffer C (25 mM Tris-HCl [pH 8.5], 150 mM KCl, 2 mM Tris(2-carboxyethyl)phosphine [TCEP] [GoldBio], 50 mM imidazole, 10% glycerol). Cleaved tags were removed by a subtractive NiNTA step. Subsequently, an anion exchange step was performed with two 5-mL HiTrap Q-FF (Cytiva Life Sciences) and protein was eluted with a KCl gradient. Eluted proteins were visualized via SDS-PAGE and select fractions were concentrated and further purified in gel filtration buffer (25 mM Tris-HCl [pH 8.0], 150 mM KCl, 1 mM TCEP, 10% glycerol) using a Superose 6 Increase 10/300 size exclusion column (Cytiva Life Sciences). Fractions were visualized by SDS-PAGE, and pure fractions were pooled, concentrated, aliquoted, flash-frozen in liquid nitrogen, and stored at −80°C until used. Protein concentration was calculated using absorbance (280 nm).

Calmodulin purification

Calmodulin (*Gallus gallus*) was recombinantly expressed from a pET-15b vector (a gift from A. Nairn, Yale School of Medicine) in BL21(DE3) cells (Millipore). Cells were grown to an OD (595 nm) of 0.6 and induced with 1 mM isopropyl β-D-1-thiogalactopyranoside (IPTG; GoldBio). Cells were grown for 16 h at 18°C and resuspended in cell lysis buffer (40 mM Tris-HCl [pH 8.0], 100 mM KCl, 10 mM EDTA). Resuspended cells were flash frozen until used. Cells were lysed via a French press, and clarified cell lysate was aspirated from cell debris following centrifugation

(18,000 rpm; 4°C; 60 min). All subsequent purification steps were performed with an ÄKTA pure chromatography system (Cytiva Life Sciences) at 4°C. Clarified cell lysate was loaded onto two 5-mL HiTrap Phenyl FF (Low Sub) columns (Cytiva Life Sciences). Column flow through was collected, and $CaCl_2$ was added to the flow through (final concentration 20 mM $CaCl_2$). The flow through was applied to a different pair of 5-mL HiTrap Phenyl FF (Low Sub) columns (Cytiva Life Sciences) with buffer A (50 mM Tris-HCl [pH 7.5], 1 mM $CaCl_2$). The column was washed sequentially with buffer A, buffer B (50 mM Tris-HCl [pH 7.5], 500 mM NaCl, 1 mM $CaCl_2$), and buffer A. Calmodulin was eluted with buffer C (50 mM Tris-HCl [pH 7.5], 2 mM EDTA). Purity was assessed via SDS-PAGE, and clean eluate fractions were pooled and concentrated. To quantify calmodulin concentration, we used circular dichroism on a Jasco J-1500 spectrophotometer to make a measurement in triplicate for our purified sample scanning a wavelength spectrum between 250 and 215 nm to measure the characteristic wavelength of 222 nm as previously described.[41] We calculated the calmodulin concentration as follows:

$$[calmodulin](nM) = \frac{1000 \times \left(CD_{sample}^{222\ nm} - CD_{blank}^{222\ nm}\right)}{\Theta \times l \times number\ of\ amino\ acids}$$

where the circular dichroism at 222 nm (CD222nm) is expressed in mdeg, Θ is the molar ellipticity, and l is the path length in cm.

Coupled kinase assay

Kinase activity was monitored under previously described conditions[40,42] with a Synergy H1 microplate reader (BioTek). Each well of the plate contained master mix composed of the following (all concentrations listed as final, working concentrations): 5 mM Tris (pH 7.5; Thermo Fisher Scientific), 150 mM KCl (Sigma), 10× Tris/$MgCl_2$ buffer (50 mM/10 mM, respectively) (Thermo Fisher Scientific), 0.2 mM $CaCl_2$ (Sigma), 1 mM phosphoenolpyruvate (Alfa Aesar), nicotinamide adenine dinucleotide (0.15 mg/mL; Sigma), pyruvate kinase (10.0 U/ml; Sigma), lactate dehydrogenase (30 U/ml; Millipore Sigma), 2.0 mM adenosine triphosphate (ATP) (Sigma), and 0.3 mM syntide (LifeTein). The final pH in each well of the reaction was ~7.5–8, and the final enzyme concentration was 13.3 nM. The reagents were added to the well in the following order: Tris buffer, calmodulin (ranging from 0.4 nM to 2 μm final concentration), and master mix. The addition of CAMK2D was used to initiate the kinase reaction, after which absorbance (340 nm) was measured at 15-s intervals for 10 min. The change in absorbance over time was fitted with a straight line (y = mx + c) to obtain a slope (m) proportional to the kinetic rate of the reaction. For each time series, slopes were fitted to a sliding window of five points (1 min 15 s), and the maximum observed slope was used to represent the kinetic rate of that reaction. Kinetic rates across a series of calmodulin concentrations were fitted with the following equation:

$$Y = Y_{min} + \frac{(Y_{max} - Y_{min}) \times X^{n_H}}{X^{n_H} + EC_{50}^{n_H}}$$

to obtain EC50 (defined as the calmodulin concentration needed to reach the half-maximal reaction velocity) and cooperativity values (Hill coefficients, n_H). Ninety-five percent confidence intervals for fit parameters (EC50 and n_H) were determined using the following bootstrap procedure. Ten thousand replicate calmodulin concentration series were generated by randomly selecting one observed kinetic rate at each measured calmodulin concentration from the set of replicates for that variant. Each generated concentration series was fit with the equation described earlier. Parameter values at the 2.5th and 97.5th quantiles of the 10,000 fits were taken as the boundaries of the 95% confidence interval.

Mice

For the *in utero* electroporation, FvB/NHanHsd females (ordered at 6–8 weeks old from Envigo) were crossed with C57Bl6/J (ordered at 6–8 weeks old from Charles River). All mice were group-housed in IVC cages (Sealsage 1145T, Tecniplast) with bedding material (Lignocel BK 8/15 from Rettenmayer) on a 12/12 h light/dark cycle in 21°C (±1°C), humidity at 40%–70% and with food pellets (801727CRM(P) from Special Dietary Service) and water available *ad libitum*. All animal experiments were approved by the Local Animal Experimentation Ethical Committee, in accordance with Institutional Animal Care and Use Committee guidelines (IRN2019-0030).

In utero electroporation

The *in utero* electroporation was done as previously described.[19] Briefly, adult pregnant female mice (FvB/NHanHsd) underwent surgery at E14.5 of gestation. After exposing the uterus, embryonic pups were injected intraventricularly with a mixture of DNA construct (1.5–3.0 μg/μL) and FastGreen (0.05%), using the Picospritzer III, after which a small electrical current was applied (five electrical square pulses of 45V; duration 50 ms/pulse; duration pulse interval 150 ms; driven by a pulse generator ECM 830, BTX Harvard Apparatus), orientating the tweezer-type pedestal with its positive pool on top of the developing somatosensory cortex. The following plasmids were electroporated: Empty vector control; $CAMK2D^{WT}$; $CAMK2D^{S79N}$; $CAMK2D^{P139L}$; $CAMK2D^{G210R}$; $CAMK2D^{Q274P}$; $CAMK2D^{R275H}$; $CAMK2D^{L291F}$. For knockdown experiments, co-transfection of different *Camk2d* shRNAs or the control shRNA with an RFP or GFP plasmid (Addgene) were electroporated. After the procedure, the mice were returned to their home cage and went naturally into labor five days post-surgery.

Perfusion and immunohistochemistry

Pups were sacrificed at the date of birth or one day after birth (P0 or P1; postnatal day 0 or 1, respectively), through cardiac perfusion with saline solution, followed by 4% PFA. After perfusion, the brains were isolated and post-fixed in 4% PFA for 1 h at room temperature. The brains were then stored overnight in 30% sucrose in 0.1M PB. Perfused brains were embedded in 14% gelatin/30% sucrose - and free-floating sections were made using a cryo-microtome (40–50 μm thick). Sections were washed in 0.1M PB and counterstained with 4′,6-diamidino-2-phenylindole solution (DAPI, 1:10,000, Invitrogen) before being mounted on glass and covered with Mowiol (Sigma). Only a selection of sections was used for counterstaining. Stained and covered brain slices were used for confocal imaging.

Confocal microscopy

All images were acquired using a LSM700 confocal microscope (Zeiss). Images for the migration analysis were taken from two to three non-consecutive sections from at least three successfully targeted animals per condition (10× objective, 0.5 zoom, 1,024 × 1,024). Images from Zeiss were converted to .tif files and cropped in such a way that each cropped image resulted in a rectangle image reaching from the IZ (intermediate zone) to the CP (cortical plate). The cropped images were vertically divided over 10 equally sized bins, having bin 1 as first bin covering the outer layer of the CP and bin 10 as the most inner area of the cropped image (IZ).

Table 1. Overview of statistical analysis on the knockdown experiments in HEK293T cells

	p value	F (df)	shRNA 1	shRNA 2	shRNA 3
***Camk2d* knockdown**	<0.0001*	(3,12) 436.1	<0.0001*	<0.0001*	<0.0001*
***Camk2a* knockdown**	0.0179*	(3,11) 5.18	0.1397	0.0086*	0.7684
***Camk2b* knockdown**	0.0617	(3,11) 3.29			

One-way ANOVA, Dunnet's multiple comparison test compared to control scramble shRNA. Asterisks (*) indicate a statistically significant difference.

The number of transfected neurons in each bin was calculated using ImageJ and used for analysis.

Statistical analysis

Protein expression in HEK293T

Image Studio Lite (v.5.2.5) was used to quantify the amount of produced protein and autophosphorylation after transfections of the *CAMK2D* constructs in HEK293T cells. The bands were fenced in order to measure the fluorescent signal and background in the drawn square (2 pixels, top and bottom). All data were corrected for background signal. Signal of the phThr287 phosphorylation band was normalized for the signal of the CAMK2D band. To determine the CAMK2D protein level, the CAMK2D band was normalized over the RFP band. All data were then normalized to the autophosphorylation or protein levels of $CAMK2D^{WT}$ overexpression, which was set at 1. All data were assumed to be normally distributed with equal variances. Two-tailed unpaired t tests were performed between $CAMK2D^{WT}$ and each *CAMK2D* variant (dual comparison). Each condition was at least transfected in triplicate, in two separate batches of cells, for a minimum sample size of n = 6. To test the specificity of the shRNAs against *Camk2d*, statistical analysis was performed with one-way ANOVA followed by Dunnett's posthoc test for multiple comparisons, comparing the conditions to the control shRNA.

Neuronal migration

All data were assumed to be normally distributed. Statistical analysis was performed on data of the first four bins of each cropped image, corresponding to the cortical plate (CP). CP is here defined as the most proximal 40% of the dorsoventral distance between the pia and ventricle (first 4 of 10 equally spaced bins). In these neuronal migration experiments, a one-way ANOVA followed by Dunnett's posthoc test for multiple comparisons was performed. In the knockdown experiments, all conditions were compared to the scramble shRNA (control). In the overexpression experiments, all conditions were compared to empty vector control and to $CAMK2D^{WT}$ overexpression. Cumulative graphs were made as visual indication of the general migration pattern but were not used for statistical analysis. For all conditions, except shRNA3, images of at least 3 separate pups (2–4 images per pup) were used for the migration analysis. For shRNA 3, images taken of 2 separate pups (3 images per pup) were used for the analysis. Statistical tests and results have been described in Tables 1, 2, 3, 4, and 5. PRISM software (Graphpad 8.0) was used for the statistical tests, p values <0.05 were considered significant.

Table 2. Overview of statistical analysis on the *in utero* electroporation experiments: Sum percentage of targeted cells in bins 1–4

	p value	F (df)
***Camk2d* knockdown (shRNA)**	<0.0001*	(3,44) 22.69
***CAMK2D* overexpression**	<0.0001*	(7,107) 51.07

One-way ANOVA. Asterisks (*) indicate a statistically significant difference.

Results

Knockdown of *Camk2d* during brain development disrupts neuronal migration

Expression of *CAMK2D* in the brain starts during early prenatal development, suggesting an important role for CAMK2D in neurodevelopment. To investigate this, we used shRNAs to silence endogenous *Camk2d* in mice. Specificity of the three shRNAs used was tested by co-transfecting mouse *Camk2d*, *Camk2a*, or *Camk2b* together with the individual shRNAs in HEK293T cells, a cell line that has very little or no endogenous production of CAMK2. A non-specific shRNA was taken along as control. All *Camk2d* shRNAs reduced CAMK2D protein levels significantly compared to control, of which shRNA 3 proved most efficient with 91.75% protein expression downgraded (Figure 1A, statistical analysis in Table 1). CAMK2A levels were slightly but significantly reduced upon co-transfection with shRNA 2, but not with shRNA 1 or 3, whereas CAMK2B levels were unaltered in all conditions (Figure 1A).

To assess the developmental role for CAMK2D, an *in utero* electroporation (IUE) was performed at E14.5 with the different *Camk2d* shRNAs and the control shRNA. In the control shRNA condition, 84.93% of all transfected cells migrated to the cortical plate (CP) at postnatal day 1 (P1). Remarkably, knockdown of *Camk2d* resulted in less than 50% of all transfected neurons migrating to the CP (Figures 1B–1D, statistical analysis in Tables 2 and 3). Additionally, we found that CAMK2D protein levels need to be tightly regulated, as overexpression of this isozyme using IUE also resulted in a migration deficit. Where in the empty vector (EV) control condition an average of 93.32% of all transfected neurons had successfully migrated to the CP, only an average of 70.77% of the neurons reached the CP

Table 3. Post-hoc analysis of the *in utero* electroporation experiments: Sum percentage of targeted cells in bins 1–4

***Camk2d* knockdown (shRNA)**	p value
Scramble shRNA (ctrl) versus shRNA 1	<0.0001*
Scramble shRNA (ctrl) versus shRNA 2	<0.0001*
Scramble shRNA (ctrl) versus shRNA 3	<0.0001*

Dunnett's multiple comparison test. Asterisks (*) indicate a statistically significant difference.

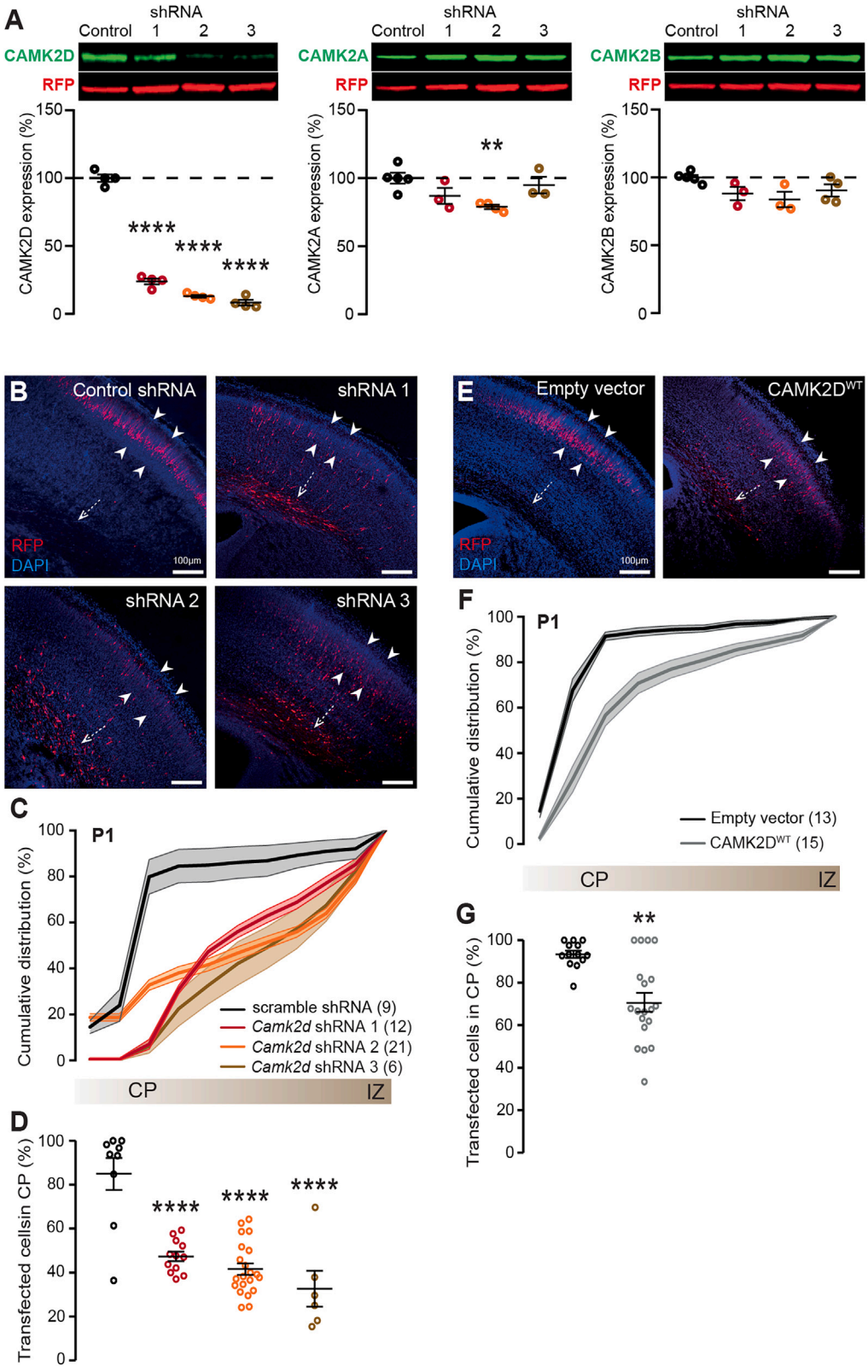

Figure 1. Reduced as well as increased CAMK2D protein level during prenatal neurodevelopment results in a migration delay
(A) Knockdown of *Camk2d* with shRNAs proves to be efficient and mostly specific. Top: representative western blots of protein lysates from HEK293T cells, which were transfected with either control (scramble) or *Camk2d* specific shRNA's. Blots were probed with an antibody against the specific CAMK2 (green), and RFP (red). Bottom: Quantification of CAMK2D (left), CAMK2A (middle), or CAMK2B (right) protein levels normalized against RFP.

(legend continued on next page)

when *CAMK2D*^{WT} was overexpressed (Figures 1E–1G, statistical analysis in Tables 2, and 5). These results indicate that CAMK2D plays a role in neurodevelopment.

Affected individuals harboring *CAMK2D* variants present with a developmental condition characterized by developmental delay/intellectual disability and cardiomyopathy

The first individual identified, individual #5 in Table 6, is a young adult woman with a congenital multiple malformations syndrome. She presented with congenital heart disease (dilated cardiomyopathy with heart failure, large ventricular septal defect requiring surgical repair), renal failure due to prolonged cardiopulmonary bypass, neurological and neurodevelopmental impairment (profound intellectual disability, almost total lack of spoken language, cerebral palsy with mixed hypotonia and hypertonia, abnormally high pain tolerance), intestinal abnormalities (Chilaiditi syndrome complicated by a megacolon, associated with dysphagia and necessitating tube feeding), compromised immune system (eosinophilic esophagitis due to atopic predisposition combined with severe allergies, asthma, eczema, rosacea), skeletal abnormalities (scoliosis, kyphosis), and strabismus. Trio-based exome sequencing highlighted a nonsynonymous *de novo* variant in *CAMK2D* (GenBank: NM_001321571.2): c.821A>C (p.Gln274Pro). Via the data sharing platform GeneMatcher[38] and direct requests in variant databases from participating centers, five additional distinct rare missense *CAMK2D* variants and one splice *CAMK2D* variant could be identified in seven individuals with neurodevelopmental disorders. Five variants were *de novo,* whereas the sixth one was present in two siblings and likely inherited from the deceased father who had similar symptoms.

Six of the seven variants are missense substitutions located in either the catalytic domain (p.Ser79Asn, p.Pro139Leu, and p.Gly210Arg) or the regulatory domain (p.Gln274Pro, p.Arg275His, and p.Leu291Phe), whereas the seventh variant is located at a splice site, potentially leading to frameshift variant (p.Val74Glufs*11) and thus to a premature truncation of the protein, or nonsense-mediated RNA decay, as a consequence of skipping of exon 4 (c.275+1G>T) (Figure 2A). Predicted conformational changes on tertiary protein structure of the missense variants are shown in Figures 2B–2G. All affected amino acid residues were absent in public exome and genome databases (gnomAD, >246,000 chromosomes; NHLBI Exome Variant Server, >13,000 alleles; Bravo, 125,568 alleles), highly conserved across species from mammals down to *Caenorhabditis elegans* and *Saccharomyces cerevisiae*, and predicted as pathogenic by bioinformatics programs compiled by MobiDetails[43] and including CADD, REVEL, SIFT, and PolyPhen 2 (Tables 6 and S3).

The main clinical features of individuals with *CAMK2D* variants are summarized in Table 6. Additional details are provided in Table S3. With the exception of individual #8 who was too young at the time of consultation to have a cognitive assessment, all other individuals had mild to profound developmental delay or intellectual disability (7/7) characterized by speech (7/7, including 4 non-verbal individuals) and motor delay (7/7, including one individual unable to walk and 3 requiring assistance to walk), as well as behavioral problems (7/7, including 4 individuals with autism spectrum disorder and 1 with attention deficit hyperactivity disorder). Brain magnetic resonance imaging performed in 5/8 individuals revealed variable structural brain abnormalities, particularly a dilatation of lateral ventricles. Hypotonia was noted in 5/8 and seizures in 2/8 of the individuals. Strikingly, all but one of the individuals identified with a missense variant had dilated cardiomyopathy (6/7), in contrast to the only individual identified with a gene disruptive variant (#1), who had no cardiac symptoms or anomalies seen by echocardiography. Cardiomyopathy was severe in all the patients concerned, and cardiac transplantation was performed or planned in most cases after failure of symptomatic treatments (including angiotensin-converting enzyme inhibitors). Almost all individuals showed dysmorphic facial features (7/8; Figure 2H). The facial analysis by GestaltMatcher[46,47] and GestaltMatcher Database[48] showed that although the facial phenotype of *CAMK2D* was not similar to *CAMK2A*, *CAMK2B*, and *CAMK2G* on the cohort level analysis, the four individuals of *CAMK2D* showed a moderate degree of facial similarity (see GestaltMatcher analysis and Figures S1 and S2). Most individuals exhibited variable skeletal malformations (7/8), involving spine, hands, feet, or palate. Additional recurrent issues were severe gastrointestinal problems—especially dysphagia—often requiring tube feeding (4/6) and correlating with low muscle tone, short stature (3/8; from −2.1 to −3.3 SD), and visual anomalies (5/5, including 2 individuals with astigmatism and individuals with either cortical vision impairment, myopia, or strabismus).

(B) Representative images of coronal brain slices from P0/P1 pups that were transfected with scramble or *Camk2d*-specific shRNAs at E14.5, using *in utero* electroporation. White dashed arrow indicates the subventricular zone (SVZ); white arrowheads indicate the cortical plate (CP). DAPI is in blue, RFP in red.
(C) Cumulative graph indicating the migration pattern from the SVZ to the CP in presence of scramble or *Camk2d*-specific shRNAs.
(D) Quantification of tdTomato-positive cells that have successfully migrated to the CP, revealing that knockdown of *Camk2d* leads to a delay in migration.
(E) Representative images of coronal brain slices from P0/P1 pups that were transfected with a control empty vector or *CAMK2D*^{WT} at E14.5, using *in utero* electroporation.
(F) Cumulative graph indicating the migration pattern from the SVZ to the CP upon overexpression of the empty vector or *CAMK2D*^{WT}.
(G) Quantification of tdTomato-positive cells that have successfully migrated to the CP, showing that overexpression of *CAMK2D*^{WT} leads to a delay in migration as well. Number in parentheses represents the number of images used for the quantification; dots represent data points and error bars indicate SEM; *$p < 0.05$; **$p < 0.01$; ****$p < 0.0001$.

Table 4. Clinical features of the individuals with variants in *CAMK2D*

	1	2	3	4	5	6	7	8	Total
Variant nomenclature chr4 (GRCh37)[a]									
Genome	g.114530307C>A	g.114530347C>T	g.114458598G>A	g.114438787C>T	g.114435068T>G	g.114435065C>T	g.114435065C>T	g.114435016C>G	7 variants 1 SS, 6 MS
Nucleotides	c.275+1G>T	c.236G>A	c.416C>T	c.628G>A	c.821A>C	c.824G>A	c.824G>A	c.873G>C	
Amino acids	p.?	p.Ser79Asn	p.Pro139Leu	p.Gly210Arg	p.Gln274Pro	p.Arg275His	p.Arg275His	p.Leu291Phe	
Variant annotation									
MobiDetails[b]	92725	93616	93619	272319	93654	93656	93656	93659	
CADD (v.1.6)	34	25.90	33	26.30	24.90	24.60	24.60	22.50	
Metadome (tolerance score)	N/A	neutral	highly intolerant	unknown	intolerant	intolerant	intolerant	highly intolerant	
MPA	10 (high splice)	6 (moderate missense)	7 (moderate missense)	7 (moderate missense)	5 (low missense)	5 (low missense)	5 (low missense)	5 (low missense)	
Revel	N/A	uncertain	damaging	damaging	uncertain	uncertain	uncertain	uncertain	
ClinPred	N/A	damaging	damaging	damaging	damaging	damaging	damaging	damaging	
Mistic	N/A	damaging	damaging	damaging	damaging	damaging	damaging	damaging	
gnomAD v.2.1.1	absent	absent	absent	absent	absent	absent	absent	absent	
ClinVar	SCV002103284	SCV002103285	SCV002103286	SCV003799177	SCV002103287	SCV002103288	SCV002103288	SCV002103289	
Mode of inheritance	*de novo*	*de novo*	*de novo*	*de novo*	*de novo*	dominant	dominant	*de novo*	
Method of mutation detection	ES	ES	ES	ES	ES	ES	ES	GS	
Gender	female	female	male	male	female	male	female	male	4 F, 3 M
Age at last investigation	11 years	2 years	4 years	6 years	20 years	12 years	17 years	5 weeks	5 weeks to 19 years
Height at age last investigation (SD)	+1.69	−1.14	−2.86	−1.37	−3.28	−0.94	−2.1	−1.14	−3.28 to −0.94
Developmental delay or ID	+; mild	+; moderate to severe	+; severe	+; severe	+; profound	+; mild	+; severe	ND	7/7
Delay in walking	+	+	+	+	+	+	+	ND	7/7
Speech delay	+	+; non-verbal	+; non-verbal	+; vocalizations only	+; non-verbal	+; mixed receptive-expressive language disorder	+; non-verbal	ND	7/7
Dysmorphic facial features	+	+	+	+	+	+	+	–	7/8

(*Continued on next page*)

Table 4. ***Continued***

	1	2	3	4	5	6	7	8	Total
Skeletal anomalies	+; hands, feet	+; spine	+; thorax	+; hands, feet, thorax, palate	+; feet, thorax	+; hands	+; hands, feet, palate	–	7/8
Dilated cardiomyopathy	–	+; cardiac transplantation	+; planned cardiac transplantation	–	+; severe, cardiac transplantation impossible; VSD repaired, PDA	+; cardiac transplantation	+; severe; AtSD and PAPVR repaired	+; severe	6/8
Abnormal muscle tone	+	+	+	+	+	–	–	–	5/8
Seizures	+	–	–	–	+	–	–	–	2/8
Behavioral anomalies	+; ASD	+; ASD	+	+	+; ASD	+; ADHD	+; ASD	ND	7/7
Digestive problems	–	+; GJ tube feeding	+; NJ feeding	+; chronic constipation	+; tube feeding, EoE, dysphagia, megacolon	ND	ND	–	4/6
Visual anomalies	+	+	ND	+	+	ND	+	ND	5/5
Urogenital/kidney anomalies	–	–	+	–	+	ND	ND	–	2/6
Anomalies in brain imaging	+; enlarged ventricles	+; enlarged ventricles	+; hemorrhagic infarcts	+; enlarged ventricles	+; decreased brain volume	ND	ND	ND	5/5
EEG anomalies	+	–	ND	+	ND	ND	ND	ND	2/3

N/A, not applicable; ND, not determined; SD, standard deviation; ES, exome sequencing; GS, genome sequencing; VSD, ventricular; AtSD, atrial septal defect septal defect; PDA, patent ductus arteriosus; ASD, autism spectrum disorder; ADHD, attention deficit/hyperactivity disorder; GJ tube feeding, gastrostomy-jejunostomy tube feeding; NJ feeding, naso-jejunal feeding; EoE, eosinophilic esophagitis; PAPVR, partial anomalous pulmonary venous return.

[a]Nomenclature HGVS v.2.0 according to mRNA reference sequence GenBank: NC_000004.11 (NM_001321579.2) for the splice site variant in individual 1 and GenBank: NM_001321579.2 for missense variants in individuals 2–9. Nucleotide numbering uses +1 as the A of the ATG translation initiation codon in the reference sequence, with the initiation codon as codon 1.

[b]For online access, insert the accession number in place of <XXX> at https://mobidetails.iurc.montp.inserm.fr/MD/api/variant/<XXX>/browser/

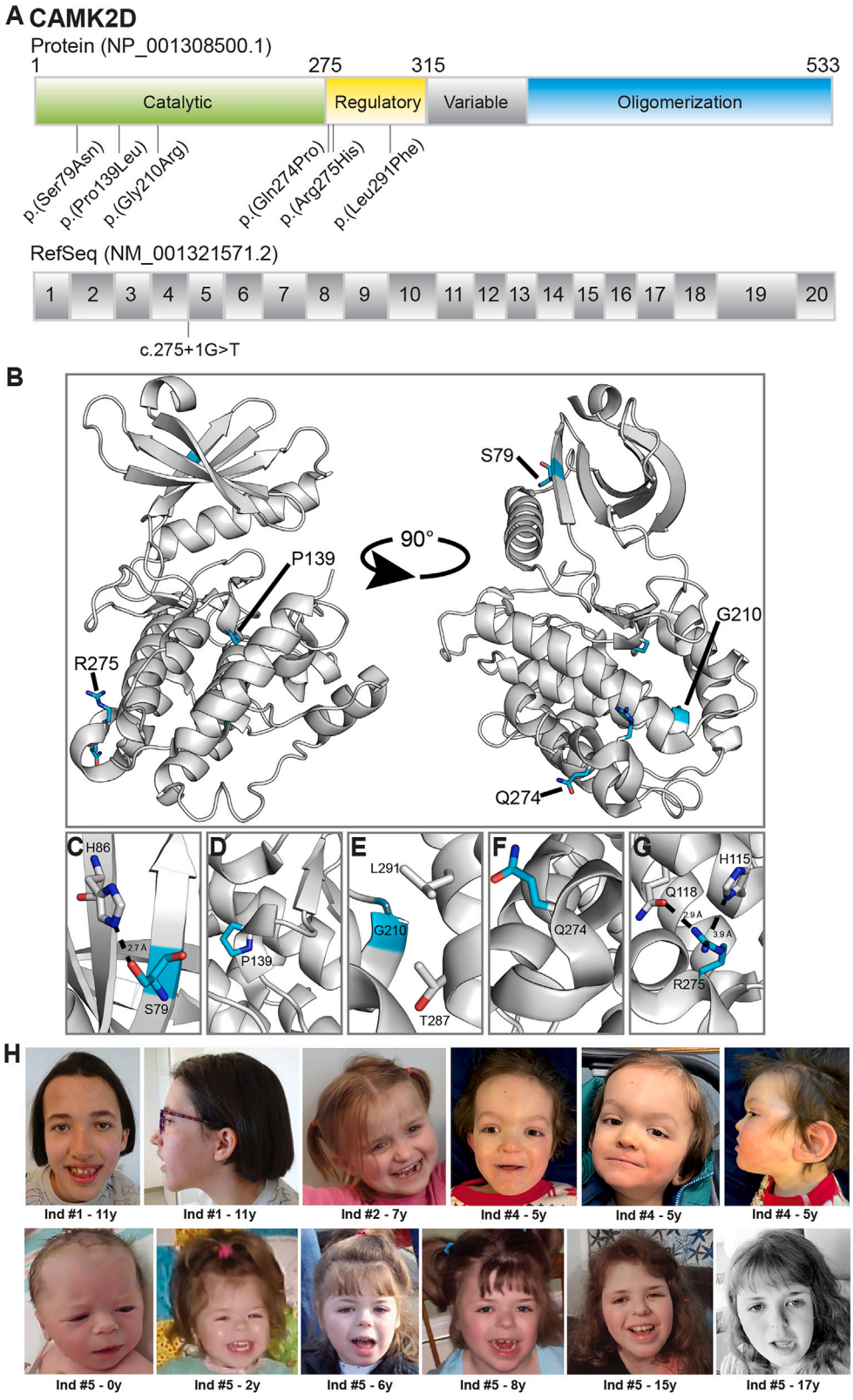

Figure 2. ***CAMK2D*** **missense variants identified in our cohort**

(A) Schematic overview of the CAMK2D protein domain organization (top) and the corresponding messenger *CAMK2D* RNA structure (bottom), showing the location of the different missense variants as well as the location of the splice site variant. Four of the variants are located in the catalytic domain (c.275+1G>T, p.Ser79Asn, p.Pro139Leu, and p.Gly210Arg) and three are located in the regulatory domain (p.Gln274Pro, p.Arg275His, and p.Leu291Phe).

(B) Crystal structure of inhibited CAMK2D and regulatory segment (PDB: 2VN9[44]), with the positions of the human variants highlighted as cyan sticks.

(legend continued on next page)

Table 5. Overview of statistical analysis on the western blot experiments for CAMK2D protein levels and Thr287 autophosphorylation

	CAMK2D expression			Thr287 phosphorylation		
	p value	df	t value	p value	df	t value
WT versus p.Ser79Asn	0.0831	50	1.768	0.0368*	51	2.145
WT versus p.Pro139Leu	0.7043	47	0.3818	0.0002*	50	4.064
WT versus p.Gly210Arg	<0.0001*	44	25.08	<0.0001*	48	7.877
WT versus p.Gln274Pro	0.0004*	47	3.813	0.0007*	57	3.566
WT versus p.Arg275His	0.0032*	47	3.112	0.0175*	59	2.446
WT versus p.Leu291Phe	<0.0001*	39	6.455	<0.0001*	43	8.059

Two-tailed unpaired t test was performed. Asterisks (*) indicate a statistically significant difference.

CAMK2D variants affect CAMK2D protein levels and kinase activity

To investigate how the variants of the eight individuals affected protein levels and/or kinase activity of CAMK2D, we expressed them in HEK293T cells and performed western blot analysis on the lysates. All data were normalized to $CAMK2D^{WT}$ expression (dotted horizontal line in Figures 3A and 3B). A significant increase in CAMK2D protein levels in HEK293T cells was observed for $CAMK2D^{Q274P}$, $CAMK2D^{R275H}$, and $CAMK2D^{L291F}$, whereas $CAMK2D^{G210R}$ showed a significant decrease, i.e., very little expression. $CAMK2D^{S79N}$ and $CAMK2D^{P139L}$ showed similar protein levels to $CAMK2D^{WT}$ (Figure 3A). Statistical analysis can be found in Table 4.

Next, we assessed the enzymatic activity of the different *CAMK2D* constructs during expression in transfected cells by using autophosphorylation at Thr287 as a readout, i.e., the ratio of autophosphorylated vs. total expression of each protein. Most of the variants revealed increased levels of phThr287, varying from a small but significant increase for $CAMK2D^{P139L}$, $CAMK2D^{Q274P}$, and $CAMK2D^{R275H}$ to a robust phThr287 increase of the small amount of $CAMK2D^{G210R}$ that is expressed (Figure 3B). Overexpressing $CAMK2D^{S79N}$ resulted in a small but significant reduction of phThr287, whereas overexpression of $CAMK2D^{L291F}$ showed very little phThr287. For statistics, see Table 4.

To further investigate the kinase activity of the $CAMK2D^{Q274P}$ and $CAMK2D^{R275H}$ variants, where the increase in autophosphorylation appeared rather mild, *in vitro* kinase assays were performed. First, similar to CAMK2A data shown previously,[32,40] a CAMK2D variant containing a 63-residue linker (6v1-14a-16-17-18, 63 aa) was more sensitive to Ca^{2+}/CaM (lower EC_{50}) compared to a CAMK2D variant containing no linker (Figure 3C). The CAMK2D-63 with an EC_{50} for Ca^{2+}/CaM of 20 nM was used to assess the effect of the human variants on kinase activity.[32] $CAMK2D^{Q274P}$ and $CAMK2D^{R275H}$ displayed slightly lower EC_{50} values of 8 nM and 11 nM, respectively (Figure 3D). These results suggest that the variants make it easier for CAMK2D to become enzymatically active, requiring lower levels of Ca^{2+}/CaM. Strikingly, $CAMK2D^{Q274P}$ showed an elevated baseline, indicating there is kinase activity in the absence of Ca^{2+}/CaM (Figure 3D). We compared the phosphorylation rates at zero Ca^{2+}/CaM and found that $CAMK2D^{Q274P}$ consistently showed a negative slope (indicating kinase activity) whereas $CAMK2D^{WT}$ and $CAMK2D^{R275H}$ did not (Figure 3E). These data suggest that under conditions where calcium levels are low, p.Gln274Pro likely has elevated activity, which would be detrimental to the cell.

Overexpression of *CAMK2D* variants *in utero* affects neuronal migration

Having shown that neuronal migration is sensitive to altered protein levels of CAMK2D, the IUE assay was used as an additional functional assessment for pathogenicity of the variants. We compared the effect of overexpression of the different *CAMK2D* variants to overexpression of $CAMK2D^{WT}$ in the IUE assay. When overexpressed during development, $CAMK2D^{P139L}$ and $CAMK2D^{G210R}$ showed severe migration deficits compared to $CAMK2D^{WT}$, with only 0.76% and 22.64% of the transfected neurons

(C) The hydroxyl side chain of Ser79 forms an electrostatic interaction with the sidechain of His86. Asn at this position would be too bulky to accommodate this interaction.
(D) Pro139 facilitates a short helical turn in the C-lobe. Substitution to Leu would disrupt this.
(E) Gly210 is located at the base of a helix directly facing the regulatory segment. Arg at this position would be too bulky and likely dislodge the regulatory segment.
(F) Gln274 is located within a helical turn. The positioning of a Pro in this helix would disrupt folding of this region.
(G) Arg275 is located within the same turn and is proximal enough to Gln118 for hydrogen bonding (2.9 Å) and His115 (3.9 Å) for like-charged pair interaction[45] between the two nitrogen atoms. Thus, substitution to a His would disrupt these interactions and the position of the alpha helix.
(H) Pictures of four individuals carrying a variant in *CAMK2D*. Note the coarse features and down-slanting palpebral fissures visible especially in individuals #2, #4, and #5, who also have a short nose and thin lips. Individual #1 has a long face with a high forehead, and she also has low-set ears, like individual #4.

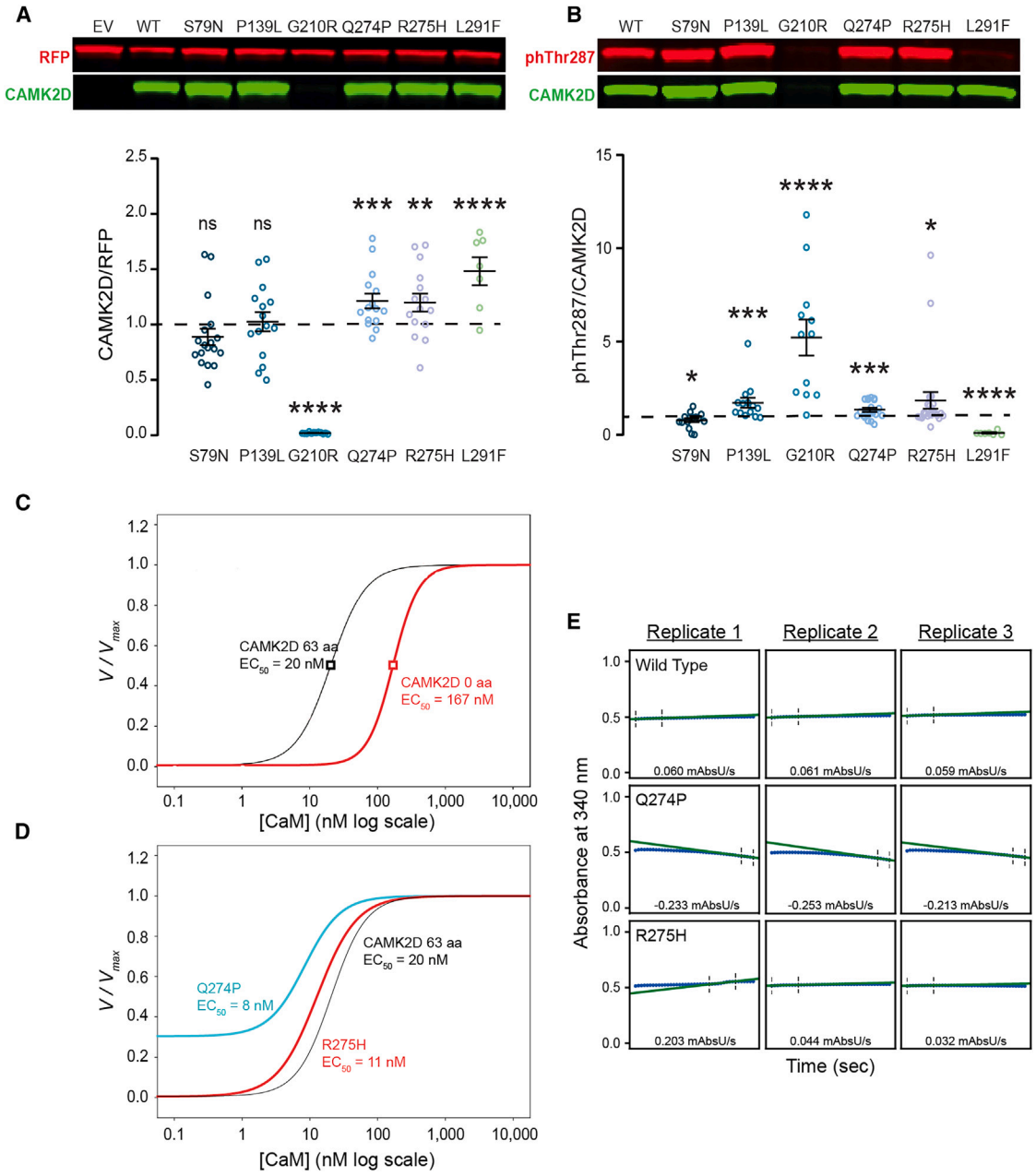

Figure 3. Assessment of protein levels and kinase activity

(A) Top: representative western blot of protein lysates from HEK293T cells that were transfected with either EV (empty control vector), *CAMK2D*^{WT}, *CAMK2D*^{S79N}, *CAMK2D*^{P139L}, *CAMK2D*^{G210R}, *CAMK2D*^{Q274P}, *CAMK2D*^{R275H}, or *CAMK2D*^{L291F}, probed with an antibody against CAMK2D (green) and RFP (red). Bottom: Quantification of CAMK2D expression normalized against RFP, showing the effects on protein of the variants. Black dashed line represents *CAMK2D*^{WT}.

(B) Top: representative western blot of protein lysates from HEK293T cells which were transfected with either EV (empty control vector), *CAMK2D*^{WT}, *CAMK2D*^{S79N}, *CAMK2D*^{P139L}, *CAMK2D*^{G210R}, *CAMK2D*^{Q274P}, *CAMK2D*^{R275H}, or *CAMK2D*^{L291F}, probed with an antibody against CAMK2D (green), phThr287 (red). Bottom: Quantification of autophosphorylated CAMK2D (phThr287) normalized against CAMK2D protein level, showing the effects on autophosphorylation of the variants. All data were normalized against level of autophosphorylation in CAMK2D^{WT}, represented by the black dashed line.

(C and D) On the y axis is the normalized rate of phosphorylation and on the x axis the respective calmodulin concentration. Data were normalized within the triplicate to the maximal rate. The hill coefficient (nH) and EC50 determined by the fits are listed below the corresponding *CAMK2D* variant for each plot. (C) Fits (see subjects and methods) of CAMK2D without linker (red) or with a 63-amino-acid linker region (black). (D) Fits of CAMK2D^{Q274P} (cyan) and CAMK2D^{R275P} (red) each with a 63-amino acid linker.

(E) Individual replicates of the coupled kinase assay in absence of CaM, to assess baseline kinase activity. A negative slope indicates increased kinase activity (blue line is the raw data; green line is the linear fit from which maximal slopes are calculated). Dots represent data points. Error bars indicate SEM; *p < 0.05; **p < 0.01; ***p < 0.001; ****p < 0.0001.

Table 6. Post-hoc analysis of the *in utero* electroporation experiments: Sum percentage of targeted cells in bins 1–4

	p value
Empty vector (ctrl) versus *CAMK2D* overexpression	
Ctrl versus WT	0.0021*
Ctrl versus p.Ser79Asn	0.9842
Ctrl versus p.Pro139Leu	<0.0001*
Ctrl versus p.Gly210Arg	<0.0001*
Ctrl versus p.Gln274Pro	<0.0001*
Ctrl versus p.Arg275His	<0.0001*
Ctrl versus p.Leu291Phe	<0.0001*
***CAMK2D*^{WT} (WT) overexpression versus *CAMK2D*^{mutant} overexpression**	
WT versus p.Ser79Asn	0.0024*
WT versus p.Pro139Leu	<0.0001*
WT versus p.Gly210Arg	<0.0001*
WT versus p.Gln274Pro	0.5225
WT versus p.Arg275His	0.1682
WT versus p.Leu291Phe	<0.0001*

Dunnett's multiple comparison test. Asterisks (*) indicate a statistically significant difference.

migrating to the outer cortical layers at P1 (Figure 4). Interestingly, CAMK2D^{S79N} significantly improved neuronal migration compared to CAMK2D^{WT}, where 98.31% of the neurons reached the CP, which is comparable to the empty vector control condition. CAMK2D^{Q274P} and CAMK2D^{R275H} showed similar behavior in the migration assay as CAMK2D^{WT}, with an average of 62.21% and 58.67%, respectively, of transfected neurons migrated to their final destination (Figure 4). For statistics, see Tables 2 and 5. An overview of the functional assessments on the *CAMK2D* missense variants can be found in Table 7.

Discussion

The CAMK2 protein family consists of four different isozymes, of which CAMK2A, CAMK2B, and CAMK2G have been shown to play a role in the human brain, causing neurodevelopmental disorders.[19,22–27] In this study, we provide evidence for a role for the CAMK2D protein in neurodevelopment. First, we show that knockdown of *Camk2d* during neurodevelopment severely disrupts the neuronal migration *in vivo,* and second, we identified eight individuals with neurodevelopmental disorders carrying variants in *CAMK2D*, all presenting with a neurodevelopmental phenotype with significant delay across all domains (cognitive, motor, speech-language) and dysmorphic facial features. Additionally, the majority of individuals presented with dilated cardiomyopathy, further emphasizing the role of CAMK2D in cardiac functioning. Similar to what has been found for *CAMK2A* and *CAMK2B*, the variants are found in the kinase domain and in the regulatory domain and cause both loss-of-function and gain-of-function effects of CAMK2D. Although the total cohort of individuals harboring variants in one of the *CAMK2* genes is small (44 published in total) and the clinical spectrum is broad, some overlapping and some unique clinical manifestations can be identified. Two common clinical manifestations seen in all CAMK2 individuals are intellectual disability, ranging from mild to profound, and delay in speech development. Similar to individuals with variants in *CAMK2D*, those associated with *CAMK2A* and *CAMK2B* variants may display seizures, brain imaging abnormalities, and digestive disorders, although this is not constant in all individuals and is more often seen with *CAMK2B* than *CAMK2A* variants.[22–24,26,27,49,50] Interestingly, the two individuals carrying the same variant in *CAMK2G* do not show seizures or abnormalities of the digestive system.[19] Distinct facial features and hypotonia have also been described for *CAMK2A, CAMK2B*, and *CAMK2G*, but again they are neither systematic nor homogeneous. Cardiac abnormalities are unique for the individuals harboring *CAMK2D* variants, as they are not found in CAMK2A-, CAMK2B-, or CAMK2G-related conditions. Identification and deep clinical phenotyping of additional individuals harboring variants in *CAMK2* genes will further clarify the differences between and specificities of the different CAMK2-related conditions.

Our functional analyses indicate that CAMK2D^{S79N} results in a possible loss of function (LoF) of CAMK2D, with slightly reduced phosphotransferase activity in HEK293T cells and improved migration compared to CAMK2D^{WT} overexpression; CAMK2D^{P139L}, CAMK2D^{G210R}, CAMK2D^{Q274P}, CAMK2D^{R275H}, and CAMK2D^{L291F} cause a GoF, all showing increased protein expression and/or phosphotransferase activity, and overexpression of CAMK2D^{P139L}, CAMK2D^{G210R}, and CAMK2D^{L291F} induced a severe migration deficit, whereas for CAMK2D^{Q274P} and CAMK2D^{R275H} this migration deficit was milder, but still significantly worse than CAMK2D^{WT} overexpression. Furthermore, CAMK2D^{Q274P} and CAMK2D^{R275H} had a reduced threshold to become enzymatically active (i.e., requiring less Ca^{2+}/CaM). The CAMK2D^{Q274P} variant revealed increased autonomous baseline activity compared to CAMK2D^{WT}, showing enzymatic activity even in the absence of Ca^{2+}/CaM. Interestingly, CAMK2D^{G210R} had increased phosphotransferase activity but was expressed poorly in HEK293T cells, suggesting protein instability. Overexpression of this variant led to a severe migration deficit, suggesting that this variant potentially disrupts the CAMK2 holoenzymes endogenously expressed in the neurons that were transfected. However, it might still be that in the individual carrying this mutation, the expression levels are so low that the net effect in this individual is a LoF instead of a GoF effect.

Our findings confirm previous results, where the residue Arg274 in CAMK2A, equivalent to Arg275 in CAMK2D, was shown to be important for autoinhibition.[51] Interestingly, Lys291 in CAMK2A, equivalent to Lys292 in

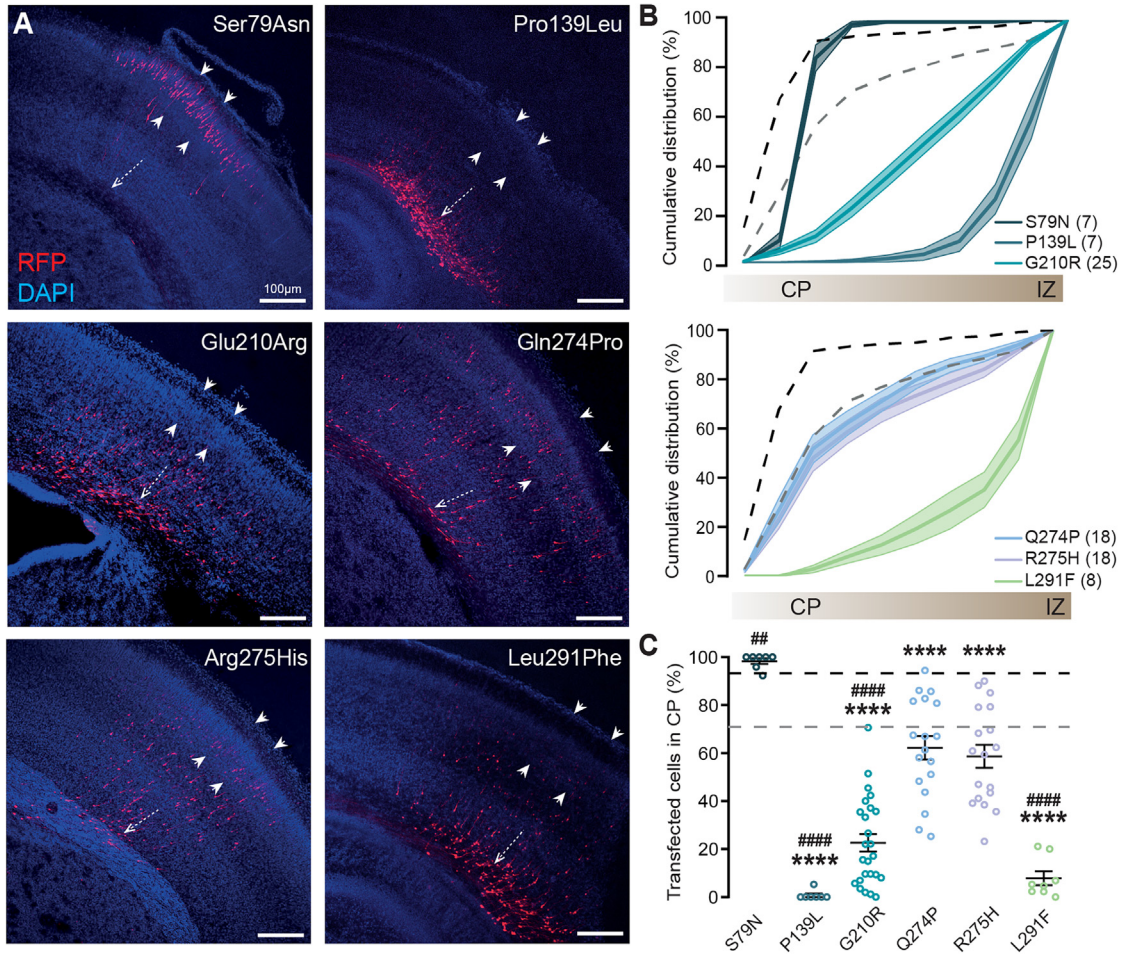

Figure 4. Overexpression of *CAMK2D* variants during prenatal neurodevelopment causes a migration deficit

(A) Representative images of coronal brain slices from P0/P1 pups that were transfected with either $CAMK2D^{S79N}$, $CAMK2D^{P139L}$, $CAMK2D^{G210R}$, $CAMK2D^{Q274P}$, $CAMK2D^{R275H}$, or $CAMK2D^{L291F}$ at E14.5, using *in utero* electroporation. White dashed arrow indicates the SVZ; white arrowheads indicate the CP. DAPI in blue, RFP in red. Scale bar indicates 100 μm.

(B) Cumulative graph indicating the migration pattern from the SVZ to the CP in presence of overexpressed $CAMK2D^{S79N}$, $CAMK2D^{P139L}$, $CAMK2D^{G210R}$, $CAMK2D^{Q274P}$, $CAMK2D^{R275H}$, or $CAMK2D^{L291F}$. Number in parentheses is the number of images used for the quantification. Black dashed line indicates EV (n = 12); gray dashed line indicates $CAMK2D^{WT}$ (n = 19) overexpression.

(C) Quantification of RFP-positive cells that have successfully migrated to the CP, showing the different effects of the variants on migration. # indicates the levels of significance compared to $CAMK2D^{WT}$ overexpression. * indicates the levels of significance compared to the empty vector control (EV). Black dashed line represents EV, gray dashed line represents $CAMK2D^{WT}$ overexpression. Dots represent data points. Error bars indicate SEM; **/##p < 0.01; ****/####p < 0.0001.

CAMK2D, right next to the p.Leu291Phe variant identified in our cohort, is also found to play a role in autoinhibition. Finally, Glu139 in CAMK2A, equivalent to Glu140 in CAMK2D, is shown to be important for substrate binding and is right next to the p.Pro139Leu variant identified in our cohort.[51] Our results suggest that residues Leu291 and Pro139 in CAMK2D have similar roles as their neighboring residues, but the exact mechanism remains to be studied. Of note, the *CAMK2D* p.Pro139Leu variant identified here is the equivalent to the *CAMK2B* p.Pro139Leu variant, which is the most recurrent variant previously identified by us and others in individuals with neurodevelopmental disorders.[26,27] Whereas neurologically the phenotypes partially overlap (severe intellectual disability, delayed speech, behavioral anomalies), affected individuals with pathogenic *CAMK2B* variants do not show cardiac anomalies, consistent with the finding that *CAMK2B* is not expressed in the heart.[52,53] *CAMK2D* p.Gln274Pro was found to have increased baseline autonomous Ca^{2+}/CaM-independent activity. The importance of this region for autonomous activity has been shown for *O*-GlcNAc-modified Ser280, a few amino acids downstream.[54] It could be hypothesized that the addition of a proline at this position alters the conformation of the CAMK2D regulatory domain so that binding to the catalytic domain necessary for autoinhibition is weakened.

CAMK2D is the major CAMK2 isozyme present in the heart[30,52] and plays an important role in cardiac function. CAMK2D activity and expression is increased upon human heart failure,[55,56] as well as upon experimentally induced heart failure.[53,57,58] Elevated CAMK2D activity and/or expression has been associated in many

Table 7. Overview of functional assessments of *CAMK2D* missense variants in molecular assays

	Protein stability compared to WT	Phosphotransferase activity compared to WT	Neuronal migration compared to WT	Inferred neuropathological mechanism
Empty vector			increased	
p.Ser79Asn	unaffected	mildly decreased	increased	loss-of-function
p.Pro139Leu	unaffected	increased	severely impaired	gain-of-function
p.Gly210Arg	severely decreased	increased	impaired	gain-of-function
p.Gln274Pro	increased	increased	similar	gain-of-function
p.Arg275His	increased	increased	similar	gain-of-function
p.Leu291Phe	increased	severely decreased	impaired	dominant negative

studies with cardiac malfunctioning. Overexpression of a nuclear isoform of *Camk2d* induces hypertrophy *in vitro* and *in vivo,*[59,60] and overexpression of a cytosolic isoform of rat *Camk2d* or human *CAMK2D* induces dilated cardiomyopathy and higher mortality,[58,61] which is alleviated by CAMK2 inhibition.[62] For arrhythmias and myocardial apoptosis, CAMK2D activation or overexpression is detrimental as well, whereas inhibition or knockdown is protective.[61,63,64] Interestingly, knockout of *Camk2d* in mice does not alter heart function under basal conditions[53,65,66] but rather protects against adverse cardiac remodeling and increases survival.[66] In a preclinical model, inducible deletion of *Camk2d* and *Camk2g* (also expressed in the heart) after heart failure slowed down the progression of cardiac dysfunction.[67] Finally, CRISPR-Cas9 gene therapy targeting *Camk2d* protected against cardiac dysfunction.[68] This is consistent with our finding, which shows that most *CAMK2D* variants associated with dilated cardiomyopathy have GoF effects, and provides a clinical validation for CAMKD hyperactivity and cardiomyopathy. The only exception is individual #2, harboring the $CAMK2D^{S79N}$ variant, who also has dilated cardiomyopathy. This variant shows a LoF effect in our functional assays. It may be that this variant has a dominant-negative effect, undetected by our functional assays, or that other factors are at play. The individuals who do not have dilated cardiomyopathy carry the variant $CAMK2D^{G210R}$ and the frameshift variant $CAMK2D^{V74E*}$. $CAMK2D^{V74E*}$ likely causes loss of protein expression, due to the premature stop, hence haploinsufficiency, which is consistent with the studies mentioned above that suggest that loss of CAMK2D is not detrimental for cardiac function. However, the lack of cardiomyopathy in individual #4 harboring the $CAMK2D^{G210R}$ variant might be more puzzling, as we find a GoF effect. We found that upon expression in HEK293T cells, the expression levels were very low. Hence the GoF effect might be overruled by the low expression levels of this protein, resulting in a significant LoF.

We describe here a role for *CAMK2D* in human brain functioning that we did not find in our literature review. Indeed, all individuals identified in this cohort show intellectual disability, delayed speech, and gross motor delay, which (because of the severity) cannot be explained by or as a consequence of their cardiac phenotype. Whether the delay in speech and walking are indeed of neurological origin or alternatively caused by affected muscle tone remains to be understood.

That this so-called non-neuronal CAMK2 protein plays a role in neurodevelopment is not completely unexpected. Whereas *CAMK2A* and *CAMK2B* are the most abundant *CAMK2* transcripts in the adult brain, during early neurodevelopment, *CAMK2D* and *CAMK2G* are the most abundant, both in rodents and humans.[19,30] Indeed, *CAMK2G* has been shown previously to play a role in neurodevelopment, with pathogenic variants causing developmental delay, severe intellectual disability, hypotonia, and facial dysmorphic features.[19] Similar clinical phenotypes are found in our *CAMK2D* cohort, described here. It could be hypothesized that the clinical phenotypes in *CAMK2D*- and *CAMK2G*-affected individuals are caused by alteration of early prenatal neurodevelopment, due to changes in early CAMK2 signaling, but that at later stages, the role of CAMK2D and CAMK2G in normal brain functioning diminishes, as CAMK2A and CAMK2B take over. For *Camk2a* and *Camk2b* it has been shown that they play an important role in the adult brain, using mouse models to induce deletion or bring back expression in adulthood.[14,69–71] Similar inducible studies have not been done yet for *Camk2d* and *Camk2g*. Hence, further research is required to gain insight into the specific roles of the CAMK2 isozymes during different stages of neurodevelopment and in the adult brain.

Taken together we report a cohort of individuals harboring variants in *CAMK2D*, presenting with neurodevelopmental disorders and dilated cardiomyopathy. Our findings further emphasize the important roles for CAMK2D in heart function and in normal brain development and function.

Appendix A

Details about the statistical tests that have been performed on results in the molecular assays can be found in Tables 1, 2, 3, 4, and 5.

Data and code availability

All variants identified are submitted to ClinVar. The functional datasets used for Figures 1, 3, and 4, supporting the current study have not been deposited in a public repository because sequences for cloning was obtained from public databases, and no public repository exist to upload raw western blot or other experimental data, but are available from the corresponding author on request.

Supplemental information

Supplemental information can be found online at https://doi.org/10.1016/j.ajhg.2023.12.016.

Acknowledgments

We would like to thank the families of the affected individuals described in this paper for their help and their willingness to contribute to this study. This research was supported by the NWO-VIDI (016.Vidi.188.014 to G.M.v.W.). Individual 8 was tested as part of the Acute Care Genomics study (GHFM76747).

Author contributions

G.M.v.W., S.K., M.M.S., and D.C.M.V. designed the study. P.M.F.R., C.d.K., M.J.D., M.P.O., E.H., C.N.J., L.A., B.Y., S.P., M.M.S., and G.M.v.W. performed functional experiments and analysis. T.-C.H., P.M.K., and M.E. performed the facial analysis. A.B. and I.M.W. performed analysis and reporting of GeneDx cases, J.A.R. and F.X. handled the Baylor Genetics cases. S.K., J.B.H., M.T., C.B., C.E.P., K.N.W., T.D.R., O.C., J.C., E.C., C.-T.F., W.W., M.M., D.B., Z.S., E.S., C.P., F.M., E.B., C.P.B., S.B., and S.M. were involved in case identification and/or data collection and contributed to the clinical information of patients. P.M.F.R., C.d.K., M.M.S., S.K., H.S., and G.M.v.W. drafted the manuscript. All authors contributed to the final version of the manuscript.

Declaration of interests

The Department of Molecular and Human Genetics at Baylor College of Medicine receives revenue from clinical genetic testing completed at Baylor Genetics Laboratories. A.B. and I.M.W. are employees of GeneDx, LLC; H.S. is a consultant for Vasa Therapeutics (Poland).

Received: April 10, 2023
Accepted: December 12, 2023
Published: January 24, 2024

Web resources

GenBank, https://www.ncbi.nlm.nih.gov/genbank/
OMIM, https://www.omim.org/

References

1. Bhattacharyya, M., Stratton, M.M., Going, C.C., McSpadden, E.D., Huang, Y., Susa, A.C., Elleman, A., Cao, Y.M., Pappireddi, N., Burkhardt, P., et al. (2016). Molecular mechanism of activation-triggered subunit exchange in Ca^{2+}/calmodulin-dependent protein kinase II. Elife *5*, e13405.
2. Lisman, J., Yasuda, R., and Raghavachari, S. (2012). Mechanisms of CaMKII action in long-term potentiation. Nat. Rev. Neurosci. *13*, 169–182.
3. Hell, J.W. (2014). CaMKII: Claiming center stage in postsynaptic function and organization. Neuron *81*, 249–265.
4. Gaertner, T.R., Kolodziej, S.J., Wang, D., Kobayashi, R., Koomen, J.M., Stoops, J.K., and Waxham, M.N. (2004). Comparative Analyses of the Three-dimensional Structures and Enzymatic Properties of α, β, γ, and δ Isoforms of Ca^{2+}-Calmodulin-dependent Protein Kinase II. J. Biol. Chem. *279*, 12484–12494.
5. Hudmon, A., and Schulman, H. (2002). Neuronal Ca^{2+}/Calmodulin-Dependent Protein Kinase II: The Role of Structure and Autoregulation in Cellular Function. Annu. Rev. Biochem. *71*, 473–510.
6. Silva, A.J., Paylor, R., Wehner, J.M., and Tonegawa, S. (1992). Impaired spatial learning in α-calcium-calmodulin kinase II mutant mice. Science *257*, 206–211.
7. Giese, K.P., Fedorov, N.B., Filipkowski, R.K., and Silva, A.J. (1998). Autophosphorylation at Thr286 of the α calcium-calmodulin kinase II in LTP and learning. Science *279*, 870–873.
8. Elgersma, Y., Fedorov, N.B., Ikonen, S., Choi, E.S., Elgersma, M., Carvalho, O.M., Giese, K.P., and Silva, A.J. (2002). Inhibitory autophosphorylation of CaMKII controls PSD association, plasticity, and learning. Neuron *36*, 493–505.
9. Silva, A.J., Stevens, C.F., Tonegawa, S., and Wang, Y. (1992). Deficient hippocampal long-term potentiation in α-calcium-calmodulin kinase II mutant mice. Science *257*, 201–206.
10. Van Woerden, G.M., Hoebeek, F.E., Gao, Z., Nagaraja, R.Y., Hoogenraad, C.C., Kushner, S.A., Hansel, C., De Zeeuw, C.I., and Elgersma, Y. (2009). βCaMKII controls the direction of plasticity at parallel fiber-Purkinje cell synapses. Nat. Neurosci. *12*, 823–825.
11. Borgesius, N.Z., van Woerden, G.M., Buitendijk, G.H.S., Keijzer, N., Jaarsma, D., Hoogenraad, C.C., and Elgersma, Y. (2011). βCaMKII plays a nonenzymatic role in hippocampal synaptic plasticity and learning by targeting αCaMKII to synapses. J. Neurosci. *31*, 10141–10148.
12. Cho, M.H., Cao, X., Wang, D., and Tsien, J.Z. (2007). Dentate gyrus-specific manipulation of β-Ca^{2+}/calmodulin-dependent kinase II disrupts memory consolidation. Proc. Natl. Acad. Sci. USA *104*, 16317–16322.
13. Bachstetter, A.D., Webster, S.J., Tu, T., Goulding, D.S., Haiech, J., Watterson, D.M., and Van Eldik, L.J. (2014). Generation and Behavior Characterization of CaMKIIβ Knockout Mice. PLoS One *9*, e105191.
14. Kool, M.J., Proietti Onori, M., Borgesius, N.Z., Van De Bree, J.E., Elgersma-Hooisma, M., Nio, E., Bezstarosti, K., Buitendijk, G.H.S., Aghadavoud Jolfaei, M., Demmers, J.A.A., et al. (2019). CAMK2-Dependent Signaling in Neurons Is Essential for Survival. J. Neurosci. *39*, 5424–5439.
15. Cohen, S.M., Suutari, B., He, X., Wang, Y., Sanchez, S., Tirko, N.N., Mandelberg, N.J., Mullins, C., Zhou, G., Wang, S., et al. (2018). Calmodulin shuttling mediates cytonuclear signaling to trigger experience-dependent transcription and memory. Nat. Commun. *9*, 2451.
16. He, X., Li, J., Zhou, G., Yang, J., McKenzie, S., Li, Y., Li, W., Yu, J., Wang, Y., Qu, J., et al. (2021). Gating of hippocampal rhythms and memory by synaptic plasticity in inhibitory interneurons. Neuron *109*, 1013–1028.e9.

17. Zalcman, G., Federman, N., Fiszbein, A., de la Fuente, V., Ameneiro, L., Schor, I., and Romano, A. (2019). Sustained CaMKII Delta Gene Expression Is Specifically Required for Long-Lasting Memories in Mice. Mol. Neurobiol. *56*, 1437–1450.
18. Ma, H., Groth, R.D., Cohen, S.M., Emery, J.F., Li, B., Hoedt, E., Zhang, G., Neubert, T.A., and Tsien, R.W. (2014). γCaMKII shuttles Ca^{2+}/CaM to the nucleus to trigger CREB phosphorylation and gene expression. Cell *159*, 281–294.
19. Proietti Onori, M., Koopal, B., Everman, D.B., Worthington, J.D., Jones, J.R., Ploeg, M.A., Mientjes, E., van Bon, B.W., Kleefstra, T., Schulman, H., et al. (2018). The intellectual disability-associated CAMK2G p.Arg292Pro mutation acts as a pathogenic gain-of-function. Hum. Mutat. *39*, 2008–2024.
20. Rigter, P.M.F., de Konink, C., and van Woerden, G.M. (2023). Loss of CAMK2G affects intrinsic and motor behavior but has minimal impact on cognitive behavior. Front. Neurosci. *16*, 1–14.
21. De Ligt, J., Willemsen, M.H., Van Bon, B.W.M., Kleefstra, T., Yntema, H.G., Kroes, T., Vulto-van Silfhout, A.T., Koolen, D.A., de Vries, P., Gilissen, C., et al. (2012). Diagnostic Exome Sequencing in Persons with Severe Intellectual Disability. N. Engl. J. Med. *367*, 1921–1929.
22. Akita, T., Aoto, K., Kato, M., Shiina, M., Mutoh, H., Nakashima, M., Kuki, I., Okazaki, S., Magara, S., Shiihara, T., et al. (2018). De novo variants in CAMK2A and CAMK2B cause neurodevelopmental disorders. Ann. Clin. Transl. Neurol. *5*, 280–296.
23. Chia, P.H., Zhong, F.L., Niwa, S., Bonnard, C., Utami, K.H., Zeng, R., Lee, H., Eskin, A., Nelson, S.F., Xie, W.H., et al. (2018). A homozygous loss-of-function CAMK2A mutation causes growth delay, frequent seizures and severe intellectual disability. Elife *7*, e32519.
24. Heiman, P., Drewes, S., and Ghaloul-Gonzalez, L. (2021). A familial case of CAMK2B mutation with variable expressivity. SAGE Open Med. Case Reports *9*, 2050313X2199098.
25. Iossifov, I., O'Roak, B.J., Sanders, S.J., Ronemus, M., Krumm, N., Levy, D., Stessman, H.A., Witherspoon, K.T., Vives, L., Patterson, K.E., et al. (2014). The contribution of de novo coding mutations to autism spectrum disorder. Nat *515*, 216–221.
26. Küry, S., van Woerden, G.M., Besnard, T., Proietti Onori, M., Latypova, X., Towne, M.C., Cho, M.T., Prescott, T.E., Ploeg, M.A., Sanders, S., et al. (2017). De Novo Mutations in Protein Kinase Genes CAMK2A and CAMK2B Cause Intellectual Disability. Am. J. Hum. Genet. *101*, 768–788.
27. Rizzi, S., Spagnoli, C., Salerno, G.G., Frattini, D., Caraffi, S.G., Trimarchi, G., Moratti, C., Pascarella, R., Garavelli, L., and Fusco, C. (2020). Severe intellectual disability, absence of language, epilepsy, microcephaly and progressive cerebellar atrophy related to the recurrent de novo variant p.(P139L) of the CAMK2B gene: A case report and brief review. Am. J. Med. Genet. *182*, 2675–2679.
28. Proietti Onori, M., and van Woerden, G.M. (2021). Role of calcium/calmodulin-dependent kinase 2 in neurodevelopmental disorders. Brain Res. Bull. *171*, 209–220.
29. Tobimatsu, T., and Fujisawa, H. (1989). Tissue-specific expression of four types of rat calmodulin-dependent protein kinase II mRNAs. J. Biol. Chem. *264*, 17907–17912.
30. Bayer, K.U., Löhler, J., Schulman, H., and Harbers, K. (1999). Developmental expression of the CaM kinase II isoforms: Ubiquitous γ- and δ-CaM kinase II are the early isoforms and most abundant in the developing nervous system. Mol. Brain Res. *70*, 147–154.
31. Srinivasan, M., Edman, C.F., and Schulman, H. (1994). Alternative Splicing Introduces a Nuclear Localization Signal That Targets Multifunctional CaM Kinase to the Nucleus. J. Cell Biol. *126*, 839–852.
32. Sloutsky, R., Dziedzic, N., Dunn, M.J., Bates, R.M., Torres-Ocampo, A.P., Boopathy, S., Page, B., Weeks, J.G., Chao, L.H., and Stratton, M.M. (2020). Heterogeneity in human hippocampal CaMKII transcripts reveals allosteric hub-dependent regulation. Sci. Signal. *13*, eaaz0240.
33. Sakagami, H., and Kondo, H. (1993). Differential expression of mRNAs encoding γ and δ subunits of Ca^{2+}/calmodulin-dependent protein kinase type II (CaM kinase II) in the mature and postnatally developing rat brain. Mol. Brain Res. *20*, 51–63.
34. Murray, K.D., Isackson, P.J., and Jones, E.G. (2003). N-methyl-d-aspartate receptor dependent transcriptional regulation of two calcium/calmodulin-dependent protein kinase type II isoforms in rodent cerebral cortex. Neuroscience *122*, 407–420.
35. Huntley, M.A., Srinivasan, K., Friedman, B.A., Wang, T.M., Yee, A.X., Wang, Y., Kaminker, J.S., Sheng, M., Hansen, D.V., and Hanson, J.E. (2020). Genome-wide analysis of differential gene expression and splicing in excitatory neurons and interneuron subtypes. J. Neurosci. *40*, 958–973.
36. Vallano, M.L., Beaman-Hall, C.M., Mathur, A., and Chen, Q. (2000). Astrocytes Express Specific Variants of CaM KII δ and γ, But Not α and β, That Determine Their Cellular Localizations. Glia *30*, 154–164.
37. Takeuchi, Y., Yamamoto, H., Fukunaga, K., Miyakawa, T., and Miyamoto, E. (2000). Identification of the Isoforms of Ca^{2+}/Calmodulin-Dependent Protein Kinase II in Rat Astrocytes and Their Subcellular Localization. J. Neurochem. *74*, 2557–2567.
38. Sobreira, N., Schiettecatte, F., Valle, D., and Hamosh, A. (2015). GeneMatcher: a matching tool for connecting investigators with an interest in the same gene. Hum. Mutat. *36*, 928–930.
39. Sloutsky, R., and Stratton, M.M. (2021). Functional implications of CaMKII alternative splicing. Eur. J. Neurosci. *54*, 6780–6794.
40. Chao, L.H., Pellicena, P., Deindl, S., Barclay, L.A., Schulman, H., and Kuriyan, J. (2010). Intersubunit capture of regulatory segments is a component of cooperative CaMKII activation. Nat. Struct. Mol. Biol. *17*, 264–272.
41. Harmat, V., Böcskei, Z., Náray-Szabó, G., Bata, I., Csutor, A.S., Hermecz, I., Arányi, P., Szabó, B., Liliom, K., Vértessy, B.G., and Ovádi, J. (2000). A new potent calmodulin antagonist with arylalkylamine structure: crystallographic, spectroscopic and functional studies. J. Mol. Biol. *297*, 747–755.
42. Barker, S.C., Kassel, D.B., Weigl, D., Huang, X., Luther, M.A., and Knight, W.B. (1995). Characterization of pp60c-src Tyrosine Kinase Activities Using a Continuous Assay: Autoactivation of the Enzyme Is an Intermolecular Autophosphorylation Process. Biochemistry *34*, 14843–14851.
43. Baux, D., Van Goethem, C., Ardouin, O., Guignard, T., Bergougnoux, A., Koenig, M., and Roux, A.F. (2021). MobiDetails: online DNA variants interpretation. Eur J Hum Genet *29*, 356–360.
44. Rellos, P., Pike, A.C.W., Niesen, F.H., Salah, E., Lee, W.H., von Delft, F., and Knapp, S. (2010). Structure of the CaMKIIδ/

Calmodulin Complex Reveals the Molecular Mechanism of CaMKII Kinase Activation. PLoS Biol. *8*, e1000426.
45. Heyda, J., Vincent, J.C., Tobias, D.J., Dzubiella, J., and Jungwirth, P. (2010). Ion specificity at the peptide bond: Molecular dynamics simulations of N-methylacetamide in aqueous salt solutions. J. Phys. Chem. B *114*, 1213–1220.
46. Hsieh, T.-C., Bar-Haim, A., Moosa, S., Ehmke, N., Gripp, K.W., Pantel, J.T., Danyel, M., Mensah, M.A., Horn, D., Rosnev, S., et al. (2022). GestaltMatcher facilitates rare disease matching using facial phenotype descriptors. Nat. Genet. *54*, 349–357.
47. Hustinx, A., Hellmann, F., Sümer, Ö., Javanmardi, B., André, E., Krawitz, P., and Hsieh, T.-C. (2023). Improving Deep Facial Phenotyping for Ultra-rare Disorder Verification Using Model Ensembles. Proc. - 2023 IEEE Winter Conf. Appl. Comput. Vision, WACV, 5017.
48. Lesmann, H., Lyon, G.J., Caro, P., Abdelrazek, I.M., Moosa, S., Pantel, J.T., Ten Hagen, M., Rosnev, S., Kamphans, T., Meiswinkel, W., et al. (2023). GestaltMatcher Database - a FAIR Database for Medical Imaging Data of Rare Disorders. Preprint at medRxiv. https://doi.org/10.1101/2023.06.06.23290887.
49. Fujii, H., Kidokoro, H., Kondo, Y., Kawaguchi, M., Horigane, S.I., Natsume, J., Takemoto-Kimura, S., and Bito, H. (2022). Förster resonance energy transfer-based kinase mutation phenotyping reveals an aberrant facilitation of Ca^{2+}/calmodulin-dependent CaMKIIα activity in de novo mutations related to intellectual disability. Front. Mol. Neurosci. *15*, 970031.
50. Dwyer, B.K., Veenma, D.C.M., Chang, K., Schulman, H., and Van Woerden, G.M. (2022). Case Report : Developmental Delay and Acute Neuropsychiatric Episodes Associated With a de novo Mutation in the CAMK2B Gene (c.328G>A p.Glu110Lys). Front. Pharmacol. *13*, 1–9.
51. Yang, E., and Schulman, H. (1999). Structural examination of autoregulation of multifunctional calcium/calmodulin-dependent protein kinase II. J. Biol. Chem. *274*, 26199–26208.
52. Tombes, R.M., Faison, M.O., and Turbeville, J.M. (2003). Organization and evolution of multifunctional Ca^{2+}/CaM- dependent protein kinase genes. Gene *322*, 17–31.
53. Kreusser, M.M., Lehmann, L.H., Keranov, S., Hoting, M.O., Oehl, U., Kohlhaas, M., Reil, J.C., Neumann, K., Schneider, M.D., Hill, J.A., et al. (2014). Cardiac CaM kinase II genes δ and γ contribute to adverse remodeling but redundantly inhibit calcineurin-induced myocardial hypertrophy. Circulation *130*, 1262–1273.
54. Erickson, J.R., Pereira, L., Wang, L., Han, G., Ferguson, A., Dao, K., Copeland, R.J., Despa, F., Hart, G.W., Ripplinger, C.M., and Bers, D.M. (2013). Diabetic hyperglycaemia activates CaMKII and arrhythmias by O-linked glycosylation. Nature *502*, 372–376.
55. Kirchhefer, U., Schmitz, W., Scholz, H., and Neumann, J. (1999). Activity of cAMP-dependent protein kinase and Ca^{2+}/calmodulin-dependent protein kinase in failing and nonfailing human hearts. Cardiovasc. Res. *42*, 254–261.
56. Hoch, B., Meyer, R., Hetzer, R., Krause, E.G., and Karczewski, P. (1999). Identification and Expression of δ-Isoforms of the Multifunctional Ca^{2+}/Calmodulin-Dependent Protein Kinase in Failing and Nonfailing Human Myocardium. Circ. Res. *84*, 713–721.
57. Colomer, J.M., Mao, L., Rockman, H.A., and Means, A.R. (2003). Pressure Overload Selectively Up-Regulates Ca^{2+}/Calmodulin-Dependent Protein Kinase II in Vivo. Mol. Endocrinol. *17*, 183–192.
58. Zhang, T., Maier, L.S., Dalton, N.D., Miyamoto, S., Ross, J., Bers, D.M., and Brown, J.H. (2003). The δC Isoform of CaMKII Is Activated in Cardiac Hypertrophy and Induces Dilated Cardiomyopathy and Heart Failure. Circ. Res. *92*, 912–919.
59. Ramirez, M.T., Zhao, X.L., Schulman, H., and Brown, J.H. (1997). The nuclear δ(B) isoform of Ca^{2+}/calmodulin-dependent protein kinase II regulates atrial natriuretic factor gene expression in ventricular myocytes. J. Biol. Chem. *272*, 31203–31208.
60. Zhang, T., Johnson, E.N., Gu, Y., Morissette, M.R., Sah, V.P., Gigena, M.S., Belke, D.D., Dillmann, W.H., Rogers, T.B., Schulman, H., et al. (2002). The Cardiac-specific Nuclear δB Isoform of Ca^{2+}/Calmodulin-dependent Protein Kinase II Induces Hypertrophy and Dilated Cardiomyopathy Associated with Increased Protein Phosphatase 2A Activity. J. Biol. Chem. *277*, 1261–1267.
61. Zhang, M., Gao, H., Liu, D., Zhong, X., Shi, X., Yu, P., Jin, L., Liu, Y., Tang, Y., Song, Y., et al. (2019). CaMKII-δ9 promotes cardiomyopathy through disrupting UBE2T-dependent DNA repair. Nat. Cell Biol. *21*, 1152–1163.
62. Zhang, M., Zhang, J., Zhang, W., Hu, Q., Jin, L., Xie, P., Zheng, W., Shang, H., and Zhang, Y. (2022). CaMKII-δ9 Induces Cardiomyocyte Death to Promote Cardiomyopathy and Heart Failure. Front. Cardiovasc. Med. *8*, 2163.
63. Wu, Y., Temple, J., Zhang, R., Dzhura, I., Zhang, W., Trimble, R., Roden, D.M., Passier, R., Olson, E.N., Colbran, R.J., et al. (2002). Calmodulin Kinase II and Arrhythmias in a Mouse Model of Cardiac Hypertrophy. Circulation *106*, 1288–1293.
64. Vila-Petroff, M., Salas, M.A., Said, M., Valverde, C.A., Sapia, L., Portiansky, E., Hajjar, R.J., Kranias, E.G., Mundiña-Weilenmann, C., and Mattiazzi, A. (2007). CaMKII inhibition protects against necrosis and apoptosis in irreversible ischemia-reperfusion injury. Cardiovasc. Res. *73*, 689–698.
65. Backs, J., Backs, T., Neef, S., Kreusser, M.M., Lehmann, L.H., Patrick, D.M., Grueter, C.E., Qi, X., Richardson, J.A., Hill, J.A., et al. (2009). The δ isoform of CaM kinase II is required for pathological cardiac hypertrophy and remodeling after pressure overload. Proc. Natl. Acad. Sci. USA USA *106*, 2342–2347.
66. Ling, H., Zhang, T., Pereira, L., Means, C.K., Cheng, H., Gu, Y., Dalton, N.D., Peterson, K.L., Chen, J., Bers, D., and Brown, J.H. (2009). Requirement for Ca^{2+}/calmodulin–dependent kinase II in the transition from pressure overload–induced cardiac hypertrophy to heart failure in mice. J. Clin. Invest. *119*, 1230–1240.
67. Kreusser, M.M., Lehmann, L.H., Wolf, N., Keranov, S., Jungmann, A., Gröne, H.J., Müller, O.J., Katus, H.A., and Backs, J. (2016). Inducible cardiomyocyte-specific deletion of CaM kinase II protects from pressure overload-induced heart failure. Basic Res. Cardiol. *111*, 65–69.
68. Lebek, S., Chemello, F., Caravia, X.M., Tan, W., Li, H., Chen, K., Xu, L., Liu, N., Bassel-Duby, R., and Olson, E.N. (2023). Ablation of CaMKIIδ oxidation by CRISPR-Cas9 base editing as a therapy for cardiac disease. Science *379*, 179–185.
69. Achterberg, K.G., Buitendijk, G.H.S., Kool, M.J., Goorden, S.M.I., Post, L., Slump, D.E., Silva, A.J., van Woerden, G.M., Kushner, S.A., and Elgersma, Y. (2014). Temporal and region-specific requirements of αCaMKII in spatial and contextual learning. J. Neurosci. *34*, 11180–11187.

70. Kool, M.J., Van De Bree, J.E., Bodde, H.E., Elgersma, Y., and Van Woerden, G.M. (2016). The molecular, temporal and region-specific requirements of the beta isoform of Calcium/Calmodulin-dependent protein kinase type 2 (CAMK2B) in mouse locomotion. Sci. Rep. *6*, 26989.

71. Rigter, P.M.F., Wallaard, I., Aghadavoud Jolfaei, M., Kingma, J., Post, L., Elgersma, M., Elgersma, Y., and van Woerden, G.M. (2022). Adult Camk2a gene reinstatement restores the learning and plasticity deficits of Camk2a knockout mice. iScience *25*, 105303.

The American Journal of Human Genetics, Volume *111*

Supplemental information

Role of CAMK2D in neurodevelopment and associated conditions

Pomme M.F. Rigter, Charlotte de Konink, Matthew J. Dunn, Martina Proietti Onori, Jennifer B. Humberson, Matthew Thomas, Caitlin Barnes, Carlos E. Prada, K. Nicole Weaver, Thomas D. Ryan, Oana Caluseriu, Jennifer Conway, Emily Calamaro, Chin-To Fong, Wim Wuyts, Marije Meuwissen, Eva Hordijk, Carsten N. Jonkers, Lucas Anderson, Berfin Yuseinova, Sarah Polonia, Diane Beysen, Zornitza Stark, Elena Savva, Cathryn Poulton, Fiona McKenzie, Elizabeth Bhoj, Caleb P. Bupp, Stéphane Bézieau, Sandra Mercier, Amy Blevins, Ingrid M. Wentzensen, Fan Xia, Jill A. Rosenfeld, Tzung-Chien Hsieh, Peter M. Krawitz, Miriam Elbracht, Danielle C.M. Veenma, Howard Schulman, Margaret M. Stratton, Sébastien Küry, and Geeske M. van Woerden

ROLE OF CAMK2D IN NEURODEVELOPMENT AND ASSOCIATED CONDITIONS

Pomme M.F. Rigter*, Charlotte de Konink*, Matthew J. Dunn …. Margaret M. Stratton, Sébastien Küry#, Geeske M. van Woerden#

Supplemental tables, methods and figures

Table S1. Primers used to isolate *CAMK2D*^{WT} from the human brain cDNA and tag it with AscI and PacI (restriction sites are indicated in capitals).

Location	Tag	Primers 5' >3'
5'	AscI	FW 5' – gaatCCGGCGCGCCaccatggcttcgaccacaacctg
3'	PacI	RV 5' – ggattcTTAATTAAttacttgatgggtactgttg

Table S2. Primers used during mutagenesis

Amino acid change	Nucleotide change	Primers 5' > 3'
p.Ser79Asn	c.236G>A	FW 5' – TATTGTGCGACTTCATGATAACATATCAGAAGAGGGCTTTC RV 5' – GAAAGCCCTCTTCTGATATGTTATCATGAAGTCGCACAATA
p.Pro139Leu	c.416C>T	FW 5' – TTCACAGGGACCTGAAGCTTGAGAATTTGCTTTTAGC RV 5' – GCTAAAAGCAAATTCTCAAGCTTCAGGTCCCTGTGAA
p.Gly210Arg	c.628G>A	FW 5' – CTCTATATTCTACTTGTGAGGTATCCACCCTTCTGGG RV 5' – CCCAGAAGGGTGGATACCTCACAAGTAGAATATAGAG
p.Gln274Pro	c.821A>C	FW 5' – CACCCATGGATCTGTCCACGTTCTACTGTTGCT RV 5' – AGCAACAGTAGAACGTGGACAGATCCATGGGTG
p.Arg275His	c. 824G>A	FW 5' – CCCATGGATCTGTCAACATTCTACTGTTGCTTCCA RV 5' – TGGAAGCAACAGTAGAATGTTGACAGATCCATGGG
p.Leu291Phe	c. 872G>T	FW 5' – GGAGACTGTGGAGTGTTGGCGCAAGTTCAATGCCC RV 5' – GGGCATTGAACTTGCGCCAACACTCCACAGTCTCC

Clinical synopsis of the patients

Individual #1 is the first child of healthy, non-consanguineous parents of Belgian ancestry. Family history shows relative macrocephaly in the mother (59 cm; +2,2 SD) and a paternal cousin of the mother with autism spectrum disorder. She was born after an uneventful pregnancy at 39 6/7 GW; the delivery was with vacuum extraction. Meconial amniotic fluid was noted. She didn't cry immediately, but recovered quickly. Her birth weight was 3750 gram, her height 51 cm. Her motor developmental milestones were delayed; she could sit at 8-9 months, she didn't crawl and started to walk unsupported at 23 months.

Her speech development was normal. She started primary school in regular education. She switched to special education, focused on her motor disability. She developed epilepsy at the age of 5,5 years, for which she is treated with Depakine. Clinically, the seizures are well-controlled; a 24 hour-EEG however still shows frequent epileptic activity. Her concentration skills, as well as motor skills appeared more impaired after the start of seizures. She started to fall frequently. A diagnosis of atactic dystonia was made. Fine motor skills are better than gross motor skills. Parents report a stagnation of her development.

Social emotional-development was abnormal; she was overly sociable to strangers, while she preferred playing alone at school. At the age of 11 years, she was diagnosed with autism spectrum disorder.

She has an obsession with food; she eats a lot and keeps asking for food. She displays no food-seeking behavior. She wears glasses because of myopia and astigmatism. Hearing tests were normal. Her sleeping pattern is normal. At the age of 11 years, multidisciplinary developmental testing showed a tIQ of 52 with a disharmonic profile with better performance in verbal comprehension and decreased performance in reasoning skills. Her verbal skills were tested at the level of 7 y and 11 months, with better expressive language compared to comprehension of language. Motor evaluation confirmed a atactic-dystonic pattern.

Clinical examination at 11.5 years showed a height of 161,9 cm (+1.69 SD), a weight of 48,85 kg (+0.91 SD) and a head circumference of 59.1 cm (+3.4 SD). Dysmorphic features comprised of a long face with high forehead, an upsweep in the frontal hair line with a local spot of frizzly hair, irregular dental implantation, small and low-set ears, long fingers and hypo- and hyperpigmentations on the forehead, upper part of the thorax and backside of the neck. A right-convex scoliosis was seen. Neurological evaluation showed asymmetry of the mouth when laughing, a broad-based gait, bilateral pes cavus, a mild tremor and dysmetria of the hands at coordination tests, impaired balance and normal reflexes. Brain MRI at the age of 8 years showed symmetric mild ventricular dilatation and periventricular white matter abnormalities.

Individual #2 is now a 7-year-old female who was born at 37 weeks gestational age via vaginal delivery after an uncomplicated pregnancy. Birth weight was 5 lb 7 oz. There was no family history of cardiomyopathy. No consanguinity. She was admitted to the hospital at 3 months of age due to respiratory distress and cardiomegaly on chest x-ray, and ultimately diagnosed with dilated cardiomyopathy with severely reduced function, and suspected non-compaction. Genetics consulted and testing for chromosomal abnormalities, dilated cardiomyopathy panel, and biochemical studies (organic acids, acylcarnitine profile, and plasma amino acids) was non-diagnostic. Physical examination was remarkable for dysmorphic facial features including midface hypoplasia, hypotonic mouth, frontal bossing, and deeply set eyes. Her exam was also significant for hypotonia. No history of seizures. Cardiac transplant was required at 6 months of age due to persistent poor cardiac function. Following her heart transplant, she had several infections and neutropenia for which she was placed on a single agent (tacrolimus) for her immunosuppression regimen. She has done well from cardiovascular perspective without signs and symptoms suggestive of high-grade allograft rejection.

Brain MRI at 10 months of age showed mild prominence of subarachnoid spaces lateral and third ventricle. Development was delayed. She sat around 7 months of age and began walking at 35 months. She was diagnosed with autism at 3.5 years of age. She receives developmental therapies and communicates in short phrases.

The patient required GJ tube feedings in infancy, and she had episodes of intermittent short segment small bowel-small bowel intussusceptions distal to the feeding tube. Currently, the tube is only

used for medications and supplemental nutrition during illness. Her growth parameters have been largely normal post -infancy, with height and weight at 5-10th and 10-25th centile, respectively. Her most recent head circumference at age 4 y 10 months was 49.5 cm (25th centile).

Exome trio study was performed at age 2 years and this revealed a de novo variant in *CAMK2D* (c.236G>A; p.Ser79Asn). Cardiac explant pathology was notable for left ventricular hypertrophy and chamber dilation, non-compaction (coarse trabeculation and endocardial fibroelastosis, smaller than usual pulmonary and aortic outflow valve circumferences, and non-uniform mitral valve free edge edema and thickening. The right ventricle was normal in size. The myocardium was generally well-ordered with mild biventricular myo-cytolytic changes and myocardial hypertrophy much more prominent in left than right ventricle.

Individual #3 is a 4 year 9-month-old boy of Ethiopian descent with global severe developmental delay who has been known to the genetics clinic since late pregnancy. His mother, 27 years old G3P1 had an uneventful pregnancy until she developed cholestasis of pregnancy at 35 weeks GA, secondary to maternal hepatitis B infection. An anatomical ultrasound was reported as normal and repeated at the time of maternal disease diagnosis. The fetal heart was abnormally enlarged, and a suspicion of transposition of the great arteries was suspected; pericardial effusion was noted. The fetal growth was estimated to be at 50th-75th%, and the biophysical profile was 6/8. A fetal echo showed biventricular cardiomyopathy, dilated RV and LV, with moderately reduced systolic function.
Myocardium appeared thickened, and ventricles globular. Abnormal filling
with monophasic inflow, both LV and RV, and increased A-wave reversal in IVC
and ductus venosus were noticed. There was moderate MR and TR, with a peak gradient of MR 45
mmHg, and TR 45 mmHg. In a follow up US, there was oligohydramnios, umbilical artery
Dopplers were reassuring, MCA Dopplers showed redistribution, and DV Dopplers showed
reversal of the A-wave. A fetal MRI confirmed cardiomegaly with no additional findings. A postnatal plan was created with immediate access to ECMO and PCICU, and the mother was delivered by C/S at 36 weeks GA. Neonatal diagnosis was dilated cardiomyopathy with biventricular noncompaction, and the baby was listed for cardiac transplant. A VAD implantation, followed by ABO incompatible heart transplantation took place at 3 weeks of age, followed by repair of ascending aorta and dilatation of the superior vena cava stenosis. Post surgery he developed chylothorax, and clot in the lower left extremity. A medical genetics consult was done at day 1 of life, but limited given the ICU admission; however, a microarray and WES trio were ordered. The CMA was reported as normal and WES as negative; *CAMK2D* was mentioned as a candidate gene, and a Genematcher submission and connection followed. Mitochondrial DNA analysis on cardiac tissue found a variant m.12880T>C (MT-ND5, p.Phe182Leu) with 16% heteroplasmy. More investigations revealed urine and buccal heteroplasmy of 19%. The same mitochondrial variant is present in an asymptomatic, maternally-related family member at a heteroplasmy level of 28%. CoQ was trialed for a while and discontinued as no improvement was noticed. Post-transplant he was followed closely, and hypotonia, distinctive facial features (not ethnic) and global developmental delay became gradually evident. Proximal renal tubulopathy resolved in the first few months of life, but mild proteinuria has persisted over time; he had recurrent respiratory infections, showed GI intolerance (had a G-tube), and failure to thrive. Global developmental delay was clear by 1 year of age when he was not able to sit independently, smiled occasionally, babbled, and cooed, but was difficult to engage. Growth parameters were at 5th % for weight, 19th % for length, and 54th % for head circumference. By 4 years 7 month his disproportionate growth showed: weight at the 40th %, height at the 2nd %, and head circumference at the 74th%. He continued to have hypotonia, and frequent URTIs that enhance his chronic vomiting (containing mucus, not feeds). He has continued to be stable from the cardiac standpoint; is able to cruise the furniture, crawl up the stairs, and is nonverbal, but makes lots of sounds. He is completely G-tube dependent for his feeds and has oral aversion. He helps with dressing, has good vision and hearing, recognizes his name and follows limited one-step commands. He appears distinctive with prominent forehead, deep-set eyes, and midface hypoplasia.

Individual #4 is now a 6 year old male who was initially referred for genetic evaluation at age 6 months due to hypotonia. Pregnancy was full term without complications, and patient was admitted to neonatal

intensive care for 5 days after birth due to maternal fever, tachypnea and apnea-like episodes. He had macrocephaly and hypotonia at birth. He began having subclinical seizures which were noted on electroencephalogram, and he was diagnosed with central hypothyroidism. Whole exome sequencing was performed which identified a variant of uncertain significance in *CAMK2D*, but compound heterozygous variants in another gene were thought to be a more likely explanation. Subsequent analysis of those variants has shown they are not causative for his findings, and that *CAMK2D* is his diagnosis. Additional clinical findings include cortical visual impairment, constipation, gastroesophageal reflux necessitating gastrostomy tube, mild sleep apnea, and brain MRI showed enlarged ventricles and thin corpus callosum. Physical examination notable for coarse facial features, large head, and low-set ears.

Individual #5 is a now young adult female who presented with multiple congenital anomalies and neurodevelopmental disorder. She has a history of congenital heart disease including a large ventricular septal defect and coarctation of aorta requiring multiple surgeries, as well as dilated cardiomyopathy with heart failure. In terms of neurodevelopment, she has profound intellectual disability and is essentially nonverbal. She has behavioral abnormalities including irritability, anxiety, and autistic features. From a neurologic standpoint, she has a history of cerebral palsy with mixed hypotonia and hypertonia, as well as epilepsy. A brain MRI was abnormal, demonstrating diffusely decreased brain volume and prominent CSF spaces. She has a history of GI abnormalities including Chilaiditi syndrome, eosinophilic esophagitis, and dysphagia which necessitated enteral nutrition. She has skeletal abnormalities including kyphoscoliosis, clinodactyly, and bilateral hallux valgus. She additionally has been noted to have strabismus, microcephaly, short stature, and dysmorphic features including midface hypoplasia with prognathism, facial asymmetry, epicanthus inversus, and downslanting palpebral fissures. She has a history of atopy including severe allergies, asthma, and eczema.

Individual #6 was initially evaluated in pediatric genetics clinic at age 10 years, after coming to attention due to his father and brother's diagnoses of dilated cardiomyopathy requiring heart transplant; his father was deceased at the time of the genetic evaluation and his brother was stable. Cardiac workup for this patient revealed dilated cardiomyopathy as well as an atrial septal defect and partial anomalous venous return (PAPVR). Review of his neurodevelopmental history was notable for developmental delays, learning disabilities, behavioral differences including ADHD, trichotillomania and repetitive behaviors. He had received early intervention services with continued serviced into school age with special education. This patient's physical exam was notable for the following: craniosynostosis that was repaired in infancy; wide, prominent forehead; alopecia secondary to trichotillomania; midface hypoplasia; hypertelorism; bulbous nose; short fourth and fifth metacarpal; and disproportionate growth including acromelic shortening.

Individual #7 was initially evaluated in pediatric genetics clinic at age 16 years, after coming to attention due to her father and brother's diagnoses of dilated cardiomyopathy requiring heart transplant; her father was deceased at the time of the genetic evaluation and her brother was stable. She was subsequently evaluated and also diagnosed with dilated cardiomyopathy at the age of 15 years. Upon genetic evaluation, additional history was reviewed and included findings of disproportionate short stature, atrial septal defect (repaired), dysmorphic facial features, myopia, developmental delay and intellectual disabilities. She attended school within a special education program in a 12:1:1 classroom. Upon exam, notable physical findings included the following: disproportionate short stature with acromelic shortening; wide, prominent forehead; midface hypoplasia; hypertelorism; bulbous nose with depressed/flat nasal bridge; short philtrum; and brachydactyly.

Individual #8 was the second child to non-consanguineous parents, delivered at 39 weeks following induction of labor for reduced fetal movements, with a birth weight was 3.6kg. He was admitted to the special care nursery for observation for 5 hours after delivery and was subsequently discharged home on day 3 of life. At 3 weeks of age he presented to the emergency department with poor feeding, vomiting and respiratory distress. He was diagnosed with dilated cardiomyopathy on echocardiogram and was transferred to the pediatric intensive care unit for further management. His condition deteriorated and he

required intubation and ionotropic support. Clinical trio genome sequencing was performed as part of the Acute Care Genomics study (Victorian Clinical Genetics Services, Australia; PMID 37291213) and identified a *de novo* missense variant, NM_001321569.1:c.873G>C, NP_001308498.1:p.Leu291Phe. He died at 8 weeks of age at home after his parents elected for palliative care.

GestaltMatcher analysis

We performed the GestaltMatcher approach (Hsieh et al. 2022; Hustinx et al. 2023) to analyze the facial similarities among the 15 individuals with *CAMK2A* (four images), *CAMK2B* (five images), *CAMK2D* (ten images), and *CAMK2G* (four images) who consented to the facial analysis (Supplementary Table 3). In addition to the *CAMK2D* individuals recruited in this study, we collected the facial photos from two publications of *CAMK2A* and *CAMK2B* (Küry et al. 2017) and *CAMK2G* (Proietti Onori et al. 2018), and one unpublished *CAMK2A* patient. With model ensemble and test-time augmentation, we encoded each image into 12 512-dimensional vectors, and the average of 12 cosine distances between two images quantified the facial phenotypic similarity between two images. When the distance is smaller, two images show higher facial phenotypic similarity, which means they are close in the phenotype space. We first performed the cohort-level analysis to validate whether the individuals of *CAMK2D* are similar to each other and similar to the other three genes. We further analyzed the similarities on the individual level.

Facial similarity of *CAMK2D*. To validate the similarities of *CAMK2D* individuals, we first calculated their mean pairwise distance and random sampled 100 times. Individuals 4 and 5 have multiple images, so we make sure the images from the individual will not be sampled together to avoid bias. The distribution is shown in Figure S1A (orange). We compared the distribution to two distributions (same and random) built from the 1,555 images from different subjects with 328 syndromes from GestaltMatcher Database (GMDB) (Lesmann et al. 2023). For each of the 328 syndromes, we randomly selected a sub-cohort and calculated the mean pairwise distance 100 times to build the "same" distribution (in blue color in Figure S1A). We further built the "random" distribution (distribution in red color in Figure S1A) by randomly sampling a sub-cohort (not limit them within the same syndrome) and calculating their mean pairwise distance 100 times. We performed a five-fold cross-validation on Receiver Operating Characteristic (ROC) analysis to obtain the threshold for distinguishing the same and random distributions. The threshold c was chosen by the highest Youden index, resulting in c=0.909, corresponding to a sensitivity of 0.862 and a specificity of 0.792. When more than 50% of the cohort's distribution is below the threshold, we classify it as having a similar facial phenotype. Ultimately, 63% of *CAMK2D* distribution was below the threshold, indicating a moderate facial gestalt presenting in *CAMK2D* individuals (Figure S1A).

Facial similarity among *CAMK2D*, *CAMK2A*, *CAMK2B*, and *CAMK2G*. We investigated the similarities between the individuals with two different disease-causing genes. We built two control distributions, the "same" and "different." The "same" distribution was built by sampling the individuals with "the same disorder" into two groups, and we calculated the mean pairwise distance between the individuals of these two groups (blue distribution in Figure S1B, C, and D). The "different" distribution was built by sampling two groups from two different disorders (red distribution in Figure S1B, C, and D). The threshold c=0.896 with a sensitivity of 0.903 and a specificity of 0.802 was obtained by the five-fold cross-validation of ROC analysis. When more than 50% of the distribution of two disorders is above the threshold, we classify them as not having similar facial phenotypes. On the other hand, when there is more than 50% of the distribution below the threshold, we classify them as having a similar facial phenotype. In Figure S1B, C, and D), when comparing to *CAMK2D*, the distributions of all the other three genes were more than 50% above the threshold (*CAMK2A*: 92.4%, *CAMK2B*: 98.9%, and *CAMK2G*: 97.8%).

We further investigated the facial similarities on the individual level by the pairwise comparison analysis. We compared 23 images of 15 individuals with *CAMK2D, CAMK2A, CAMK2B, and CAMK2G* to 7,459 images with 449 different disorders from GMDB by performing the leave-one-out cross-validation to simulate the real-world scenario. For example, by testing the image of Ind 5-4, we put the remaining 22 images in the space with the other 7,459 images and calculated the ranks of 22 images to Ind 5-4. With this analysis, we could visualize the similarity of each pair of individuals compared to the control cohort. Figure S2 shows that Ind 4-1 was at the 48th closest position to Ind 5-4. Moreover, G2-1 was in the 31st position to Ind 4-1, and A-1 was in the 13th position to Ind 5-6.

Therefore, with all the results, although the facial phenotype of *CAMK2D* was not similar to *CAMK2A*, *CAMK2B*, and *CAMK2G* on the cohort level analysis, some pairs of individuals still showed a high degree of similarity, such as (Ind 4-1 and G-1) and (Ind 5-6, A-1). In addition, the four individuals of *CAMK2D* showed a moderate degree of facial similarity. However, more images from different individuals might be required in the future for the comprehensive analysis of a larger cohort.

Table S3. The cohort in GestaltMatcher analysis. GMDB patient ID and photo ID can be used to visualize the photo in GMDB. The label is the ID used in Figure S2. The labels of the CAMK2D images are the same as those in Figure 2H.

GMDB Patient ID	GMDB Photo ID	Label	Gene	Variant	PMID or source
3202	4415	A1	CAMK2A	p.(Glu109Asp)	29100089
3203	4417	A2	CAMK2A	p.(Pro212Leu)	29100089
3204	4419	A3	CAMK2A	p.(Pro235Leu)	29100089
7277	11641	A4	CAMK2A	p.(Gly301Glu)	Unpublished
3205	4420	B1	CAMK2B	p.(Arg29*)	29100089
3206	4426	B2	CAMK2B	p.(Glu110Lys)	29100089
3207	4428	B3	CAMK2B	p.(Pro139Leu)	29100089
3208	4431	B4	CAMK2B	p.?	29100089
3209	4438	B5	CAMK2B	p.Lys301Glu	29100089
6686	10342	Ind 1	CAMK2D	p.?	This paper
9686	15622	Ind 2	CAMK2D	p.(Ser79Asn)	This paper
9550	15189	Ind 4-1	CAMK2D	p.(Gly210Arg)	This paper
9550	15190	Ind 4-2	CAMK2D	p.(Gly210Arg)	This paper
6685	10325	Ind 5-1	CAMK2D	p.(Gln274Pro)	This paper
6685	10327	Ind 5-2	CAMK2D	p.(Gln274Pro)	This paper
6685	10332	Ind 5-3	CAMK2D	p.(Gln274Pro)	This paper
6685	10330	Ind 5-4	CAMK2D	p.(Gln274Pro)	This paper
6685	10335	Ind 5-5	CAMK2D	p.(Gln274Pro)	This paper
6685	10336	Ind 5-6	CAMK2D	p.(Gln274Pro)	This paper
3210	4445	G1-1	CAMK2G	p.(Arg292Pro)	30184290
3210	4446	G1-2	CAMK2G	p.(Arg292Pro)	30184290

9663	15490	G2-1	CAMK2G	p.(Arg292Pro)	30184290
9663	15492	G2-2	CAMK2G	p.(Arg292Pro)	30184290

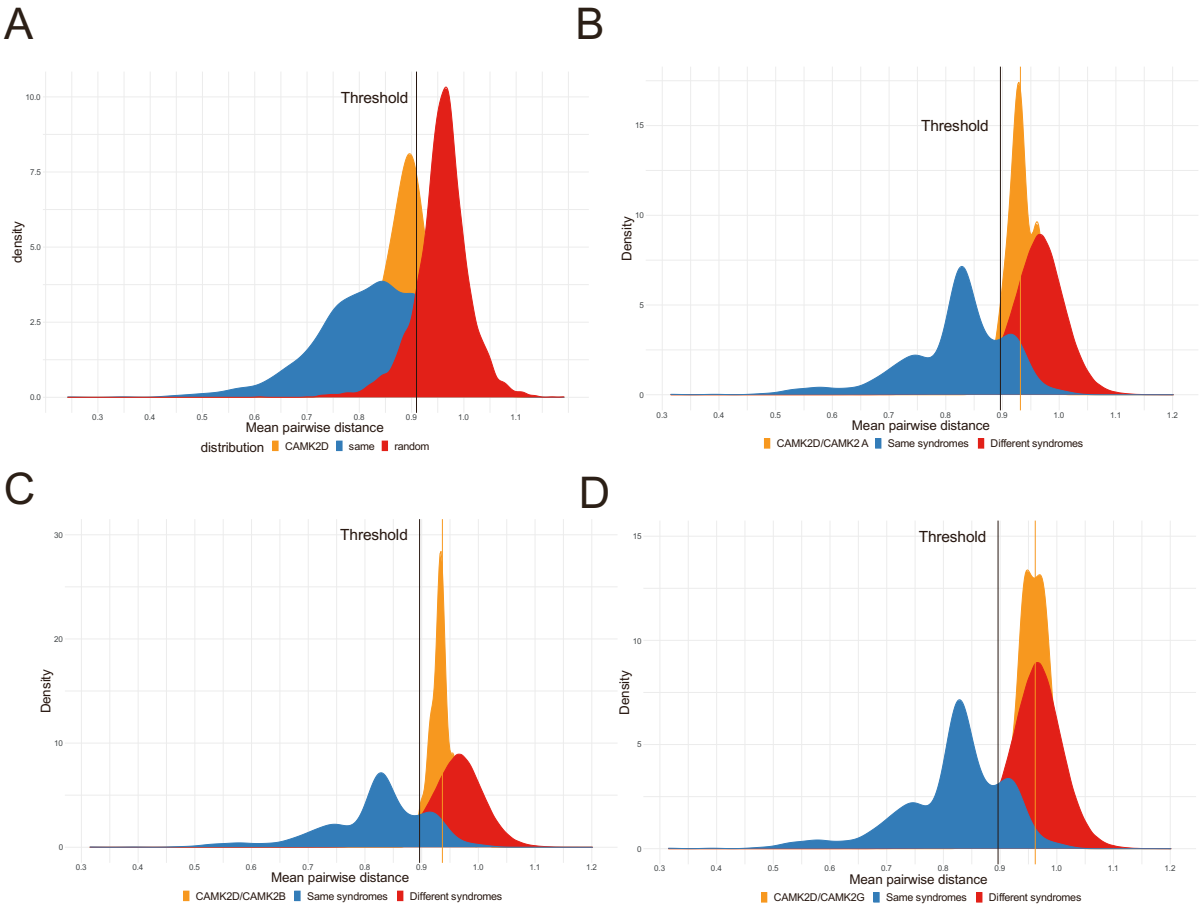

Figure S1. A) The distribution of mean pairwise distance. It shows three distributions: *CAMK2D* (orange), the random selection from the subjects with 328 disorders (red), and the selection with the same disorder (blue). The black vertical line is the threshold that classifies whether it is the same disorder or random selection. 63% of *CAMK2D* distribution are below the threshold; B) The mean pairwise distance distribution when comparing two groups: sampling from *CAMK2D and CAMK2A* (orange), sampling with the same disorder (blue), and sampling from two different disorders (red); C) orange distribution is sampled from *CAMK2D and CAMK2B*; D) orange distribution is sampled from *CAMK2D and CAMK2G*.

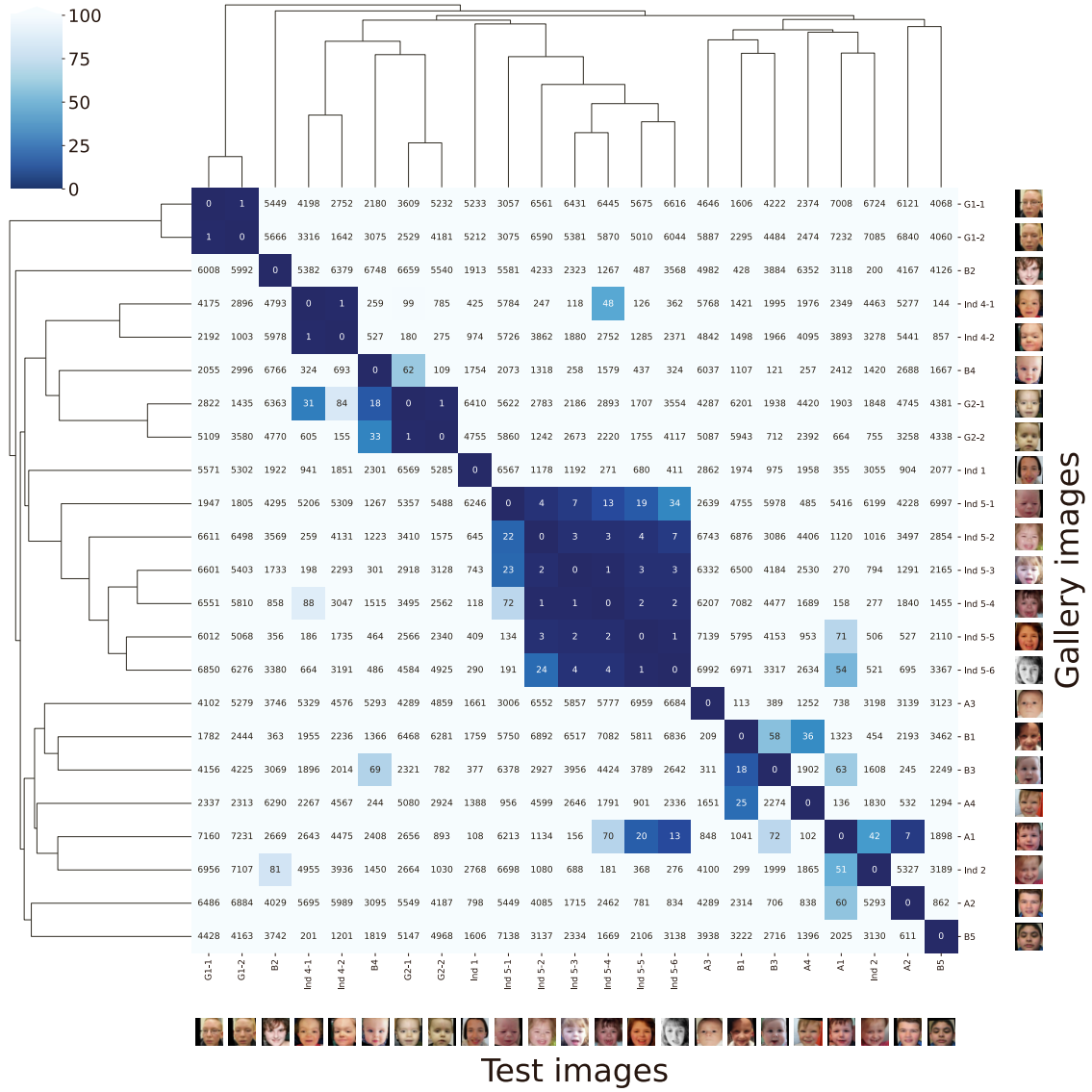

Figure S2. The pairwise rank matrix and hierarchical clustering of 23 images of 15 individuals with *CAMK2A, CAMK2B, CAMK2D* and *CAMK2G*. Each column is the result of testing one subject in the column and listing the rank of the rest of the 21 images in each row. For example, by testing Ind 5-4, Ind 4-1 was on the 48th rank, and G2-1 was on the 31st rank of Ind 4-1.

References:

Hsieh, Tzung-Chien, Aviram Bar-Haim, Shahida Moosa, Nadja Ehmke, Karen W. Gripp, Jean Tori Pantel, Magdalena Danyel, et al. 2022. “GestaltMatcher Facilitates Rare Disease Matching Using Facial Phenotype Descriptors.” *Nature Genetics* 54 (3): 349–57.

Hustinx, Alexander, Fabio Hellmann, Omer Sumer, Behnam Javanmardi, Elisabeth Andre, Peter Krawitz, and Tzung-Chien Hsieh. 2023. “Improving Deep Facial Phenotyping for Ultra-Rare Disorder Verification Using Model Ensembles.” In *2023 IEEE/CVF Winter Conference on Applications of Computer Vision (WACV)*. IEEE. https://doi.org/10.1109/wacv56688.2023.00499.

Küry, Sébastien, Geeske M. van Woerden, Thomas Besnard, Martina Proietti Onori, Xénia Latypova, Meghan C. Towne, Megan T. Cho, et al. 2017. “De Novo Mutations in Protein Kinase Genes CAMK2A and CAMK2B Cause Intellectual Disability.” *American Journal of Human Genetics* 101 (5): 768–88.

Lesmann, Hellen, Gholson J. Lyon, Pilar Caro, Ibrahim M. Abdelrazek, Shahida Moosa, Jean Tori Pantel, Merle ten Hagen, et al. 2023. “GestaltMatcher Database - a FAIR Database for Medical Imaging Data of Rare Disorders.” *MedRxiv*. https://doi.org/10.1101/2023.06.06.23290887.

Proietti Onori, Martina, Balwina Koopal, David B. Everman, Jessica D. Worthington, Julie R. Jones, Melissa A. Ploeg, Edwin Mientjes, et al. 2018. “The Intellectual Disability-Associated CAMK2G p.Arg292Pro Mutation Acts as a Pathogenic Gain-of-Function.” *Human Mutation* 39 (12): 2008–24.